Precambrian Research 359 (2021) 106181

Contents lists available at ScienceDirect

Precambrian Research

journal homepage: www.elsevier.com/locate/precamres

Reconstruction of oceanic redox structures during the Ediacaran-Cambrian transition in the Yangtze Block of South China: Implications from Mo isotopes and trace elements

Yaowen Wu [a,b], Hui Tian [a,d,*], Jie Li [c,d], Tengfei Li [a,d], Sui Ji [a,d]

[a] State Key Laboratory of Organic Geochemistry, Guangzhou Institute of Geochemistry, Chinese Academy of Sciences, Guangzhou 510640, China
[b] University of Chinese Academy of Science, Beijing 100049, China
[c] State Key Laboratory of Isotope Geochemistry, Guangzhou Institute of Geochemistry, Chinese Academy of Sciences, Guangzhou 510640, China
[d] CAS Center for Excellence in Deep Earth Science, Guangzhou 510640, China

ARTICLE INFO

Keywords:
Mo isotope
Restricted basin
Black shales
Redox conditions
Yangtze Block

ABSTRACT

To explore paleo-ocean redox variations and Mo biogeochemistry across the Ediacaran–Cambrian transition (E-C), continuous fresh core shale samples of Ediacaran to Cambrian were collected from a well drilled in the upper slope region of the Yangtze Block in South China and analyzed for $\delta^{98/95}$Mo and $\delta^{13}C_{org}$ values, TOC, as well as the concentrations of trace and rare earth elements. The Mo–U covariations, Th/U and Re/Mo ratios as well as published iron speciation data indicate a redox stratified ocean with oxic surface waters and anoxic/euxinic deep waters prevailing across the E-C transition. During the time of Cambrian Fortunian and Stage 2, the bottom water in the upper slope became oxic due to the deepening oxycline. Afterwards, widespread anoxia and/or euxinia occurred during latest Age 2 and early Age 3. The Mo concentrations and Mo/TOC ratios suggest that the Yangtze Block was well connected with the open ocean during the late Ediacaran, and then became strongly restricted at the beginning of Cambrian. Following a large-scale transgression during Cambrian Age 2, its connection with the open ocean was enhanced again. The negative $\delta^{98/95}$Mo values may reflect preferential adsorption of isotopically light Mo by Mn oxides particles above the chemocline and their subsequent shuttling to euxinic sediments in the redox stratified late Ediacaran ocean; whereas the relatively low $\delta^{98/95}$Mo values during the Cambrian Fortunian and Age 2 indicate the decrease of $\delta^{98/95}Mo_{Seawater}$ values in the restricted basin. The operation of local Mn particulate shuttles could also be stimulated by inflow of oxic waters into restricted basin during marine transgression, resulting in negative $\delta^{98/95}$Mo values. In conjunction with previous published Mo isotope data, the variations of sedimentary $\delta^{98/95}$Mo values from shallow shelf to deepwater slope regions draw the outline of 'sandwich'-like model with euxinic waters (e.g., $[H_2S]_{aq} > 11$ μM) sandwiched by oxic surface waters and anoxic deep waters during the E-C transition. The shuttling of isotopically light Mo to euxinic sediments by Mn oxides in the redox stratified Ediacaran-Cambrian ocean may play a role in driving heterogeneous heavy seawater Mo isotopes and variable sedimentary $\delta^{98/95}$Mo values.

1. Introduction

The Ediacaran–Cambrian transition (E-C) was a key time interval in Earth history that witnessed remarkable biological, oceanic, and geochemical changes (Knoll and Carroll, 1999; Kimura and Watanabe, 2001; Amthor et al., 2003; Marshall, 2006; Jiang et al., 2009; Zhang et al., 2019). Several lines of available geochemical evidence suggest that the stepwise oxygenation of the global ocean may have taken place during the late Ediacaran and triggered the diversification of Cambrian metazoans (Fike et al., 2006; Canfield et al., 2007; Scott et al., 2008; Och and Shields-Zhou, 2012; Sahoo et al., 2016; Zhang et al., 2019). However, there are also geochemical proxies, including trace metal abundance, iron speciation as well as sulfur isotopes, that support the persistence of anoxic/ferruginous deep waters across the Ediacaran-Cambrian transition, particularly in the Yangtze Block of South China (Goldberg et al., 2007; Canfield et al., 2008; Wang et al., 2012; Och et al., 2013; Pi et al., 2013; Sperling et al., 2015).

In recent decades, molybdenum (Mo) isotopes of sedimentary rocks

* Corresponding author at: #511 Kehua Road, Tianhe District, Guangzhou City, Guangdong Province, China.
E-mail address: tianhui@gig.ac.cn (H. Tian).

https://doi.org/10.1016/j.precamres.2021.106181
Received 24 July 2020; Received in revised form 8 March 2021; Accepted 11 March 2021
Available online 11 April 2021

have been effectively used to trace the local marine redox variations and/or the oxygenation state of global paleo-oceans because of its redox-sensitive nature (Siebert et al., 2003; Anbar, 2004; Arnold et al., 2004; Wille et al., 2007; Dahl et al., 2010; Wen et al., 2011; Chen et al., 2015b; Kendall et al., 2015; Ruebsam et al., 2017; Yin et al., 2018). In modern seawater, Mo is present primarily as oxyanions molybdate (MoO_4^{2-}), and the Mo concentration in seawater is uniform due to its longer residence time (440 kyr) relative to the ocean mixing time (1–2 kyr) (Collier, 1985; Miller et al., 2011). The modern seawater holds a uniform $\delta^{98/95}$Mo value of +2.3‰ (Siebert et al., 2003), which is much heavier than the $\delta^{98/95}$Mo value of riverine influx from oxidative weathering (avg. +0.7‰, Archer and Vance, 2008). More recently, King and Pett-Ridge (2018) illustrated that riverine Mo delivered to oceans may be isotopically lighter and similar to the Mo isotope range of the average continental crust (0.35–0.60‰, Willbold and Elliott, 2017). The heavy $\delta^{98/95}Mo_{Seawater}$ is mainly attributed to the preferential adsorption of isotopically light Mo by iron and/or manganese oxides under widespread oxic waters, which leads to a large isotopic fractionation ($\Delta^{98/95}Mo_{Sediment–Seawater}$) up to –3‰ between sediment and seawater (Barling et al., 2001; Goldberg et al., 2009). Under euxinic conditions with high concentrations of aqueous H_2S ($[H_2S]_{aq} > 11$ μM), all the molybdate (MoO_4^{2-}) in seawater can be converted to tetrathiomolybdate (MoS_4^{2-}) and hence transferred quantitatively into oceanic sinks with almost no isotopic fractionations (i.e., $\Delta^{98/95}Mo_{Sediment–Seawater} = \sim 0‰$, Neubert et al., 2008; Poulson Brucker et al., 2009). Under lower aqueous H_2S abundances, sedimentary Mo isotopes are highly variable due to incomplete conversion of molybdate (MoO_4^{2-}) into oxythiomolybdate species ($MoO_{4-x}S_x^{2-}$, x = 1–4) (Helz et al., 1996; Barling et al., 2001). Within the scatter, however, there does seem to be a somewhat constant average offset of about 0.7‰ (Poulson Brucker et al., 2009, and their Fig. 6). It is worthy to mention here that transferring of seawater $\delta^{98/95}$Mo values to sediments today is dependent not solely on local $[H_2S]_{aq}$ availability in the water column, but also equally affected by bottom water Mo availability (Kendall et al., 2017). It is for this reason that seawater $\delta^{98/95}$Mo values are only transferred to sediments today in strongly restricted euxinic environments with minimized Mo inputs (Kendall et al., 2017; Ostrander et al., 2020). Therefore, the sedimentary $\delta^{98/95}$Mo isotopes usually reflect the minimum $\delta^{98/95}$Mo isotopes of their contemporaneous seawater, i.e., $\delta^{98/95}Mo_{Sediment} \leq \delta^{98/95}Mo_{Seawater}$ (Dahl et al., 2010). The spatial heterogeneity of seawater Mo isotopes due to local riverine influx in restricted/semi-restricted marginal marine basins may also have an impact on the sedimentary $\delta^{98/95}$Mo values (Ruebsam et al., 2017).

Although Mo isotopes can be potentially used to reconstruct the oceanic oxygenation state and redox conditions during the Ediacaran-Cambrian transition, there are still some controversial results (Kendall et al., 2015; Cheng et al., 2018; Ostrander et al., 2019). For instance, the near-modern seawater $\delta^{98/95}$Mo values (≥2.0‰) were recorded in the Ediacaran-Cambrian euxinic black shales in the Yangtze Block, which suggests an extensive well-oxygenated ocean (Chen et al., 2015b; Kendall et al., 2015). It is worthy to note that the near-modern seawater $\delta^{98/95}$Mo values are reported only for a few samples from discrete intervals of the upper Doushantuo Formation, probably reflecting a short-term or transient oxidation of global paleo-ocean (Kendall et al., 2015). But this inference is contrary to the widespread anoxic/euxinic waters evidenced by iron speciation and sulfur isotopes during this period (Wang et al., 2012; Feng et al., 2014; Sperling et al., 2015). It would be plausible that the oceans redox state was heterogeneous and/or highly variable in space and time during the latest Ediacaran, and fluctuating redox conditions at a timescale longer than the residence time of Mo may also be responsible for the repetitive perturbations of Mo cycle (Zhang et al., 2017). Moreover, the presence of negative molybdenum isotope excursions (<–1‰) in the late Ediacaran euxinic black shales and high $\delta^{98/95}$Mo values (> +2‰) in the Lower Cambrian oxic sediments (Wen et al., 2015; Ostrander et al., 2019) are also inconsistent with the observations of modern marine systems. In addition, most $\delta^{98/95}$Mo values reported for the Ediacaran-Cambrian samples were determined from outcrop sections that may have been somewhat weathered, and some authors have suggested that the isotopically light Mo may be preferentially retained by adsorption during weathering, resulting in relatively low $\delta^{98/95}$Mo values in these weathered samples (Archer and Vance, 2008; Pearce et al., 2008; Siebert et al., 2015).

In this study, we selected fresh core samples with high stratigraphic resolution from Well ZK4411 that provide a continuous record of the upper slope sediments deposited from the late Ediacaran to the Cambrian Age 3 in the Yangtze Block. All samples were analyzed for $\delta^{98/95}$Mo values, organic carbon isotopic values ($\delta^{13}C_{org}$), total organic carbon (TOC), as well as trace and rare earth elements concentrations. In conjunction with previous studies, paleo-ocean Mo biogeochemistry and redox structure were explored, based on which an integrated evolutional model was proposed across the Ediacaran-Cambrian transition in the Yangtze Block.

2. Geological setting

2.1. Paleogeography and lithostratigraphy

The Yangtze Block is bounded by the Qinling-Dabie orogenic belt to the north, the Red River Fault Zone to the southwest, and the Xianshuihe Fault Zone to the west, as well as the Cathaysia Block to the southeast (Shu, 2012; Charvet, 2013). Following the Neoproterozoic rift events, the Yangtze Block evolved from a rift basin into a passive continental margin basin during the E–C transition (Wang and Li, 2003), and the sedimentary facies varied from shallow water carbonate facies in the interior platform, through transitional facies, to the deep water slope and basin facies in southeast region (Steiner et al., 2001; Chen et al., 2009) (Fig. 1). The shallow shelf E–C successions include the shales of Upper Ediacaran Doushantuo Formation and the dolomites of Upper Ediacaran Dengying Formation that is unconformably overlain by the thick organic-rich Lower Cambrian black shales. In regions of deep water slope to basin facies, the E–C successions include the Upper Ediacaran Doushantuo Formation and the Ediacaran to Cambrian Liuchapo Formation that is composed mainly of cherts with a thin layer of dolomites and usually conformably overlain by the Cambrian Niutitang Formation black shales.

The Upper Ediacaran Doushantuo Formation is commonly divided into four members from bottom to top (members I to IV) and the widespread 10-m-thick organic-rich black shales of member IV are considered as the regional stratigraphic marker layer (Jiang et al., 2011). Following the northwestward marine transgression during Cambrian Age 2, widespread polymetallic Ni–Mo–PGE–Au sulfide ore layers with a thickness of 3–5 cm were formed in the lowermost part of the Niutitang Formation along a 1,600 km long, narrow NE-striking belt (Jiang et al., 2006; Xu et al., 2013), and the polymetallic layer usually acts as a marker horizon for statigraphic correlation across the margin of the Yangtze platform (Pi et al., 2013; Chen et al., 2015a; Gao et al., 2016; Jin et al., 2016). Meanwhile, the contemporaneous Niutitang V-rich layers are mainly distributed in regions of deepwater slope and basin facies and usually have a thickness of 1–3 m (Chen et al., 2015a; Fu et al., 2016).

The Well ZK4411 is located in the northeast of Yinjiang County, ~270 km northeast of Guiyang City in Guizhou Province and lied in the upper slope region of the Yangtze platform during the E-C transition. The penetrated sedimentary successions, from bottom to top, include the Upper Ediacaran Doushantuo Formation, the Upper Ediacaran to Lower Cambrian Liuchapo Formation and the Lower Cambrian Niutitang Formation. The fourth member of the Doushantuo Formation (Member IV) is composed of organic-rich black shales (~10 m); the 45-m-thick Liuchapo Formation conformably overlies the Doushantuo Formation and is composed mainly of cherts with thin layers of dolomite (~6 m) and organic-rich shales (~1 m) at the base; the overlying Niutitang Formation is lithologically dominated by organic-rich black shales (~95 m)

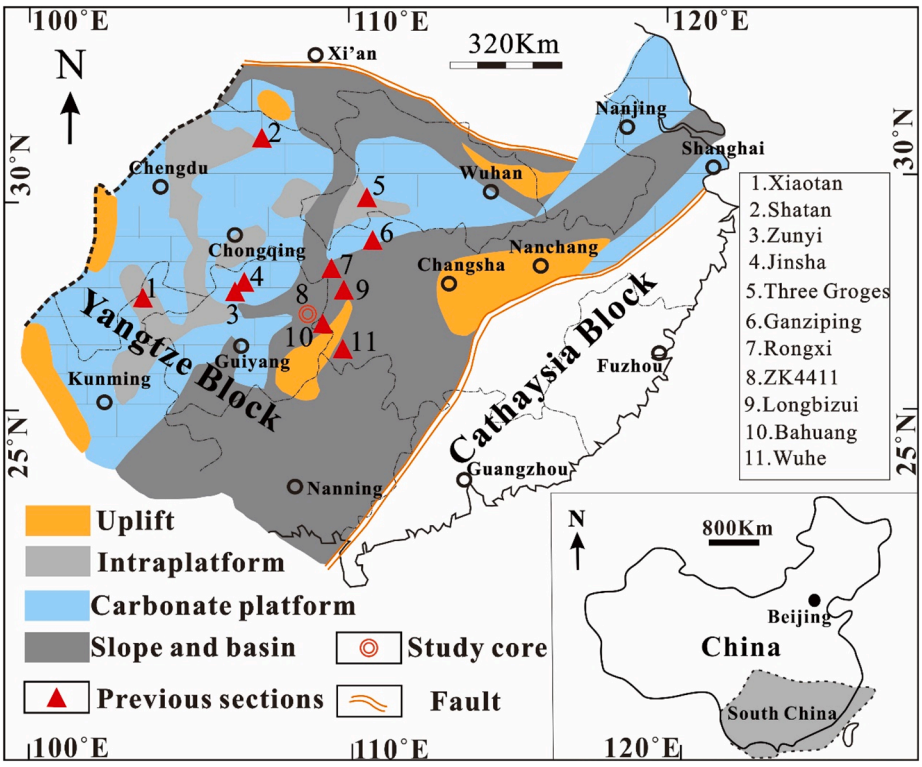

Fig. 1. Simplified paleogeographic map showing the Yangtze Block during the E-C transition (modified after Yeasmin et al., 2017).

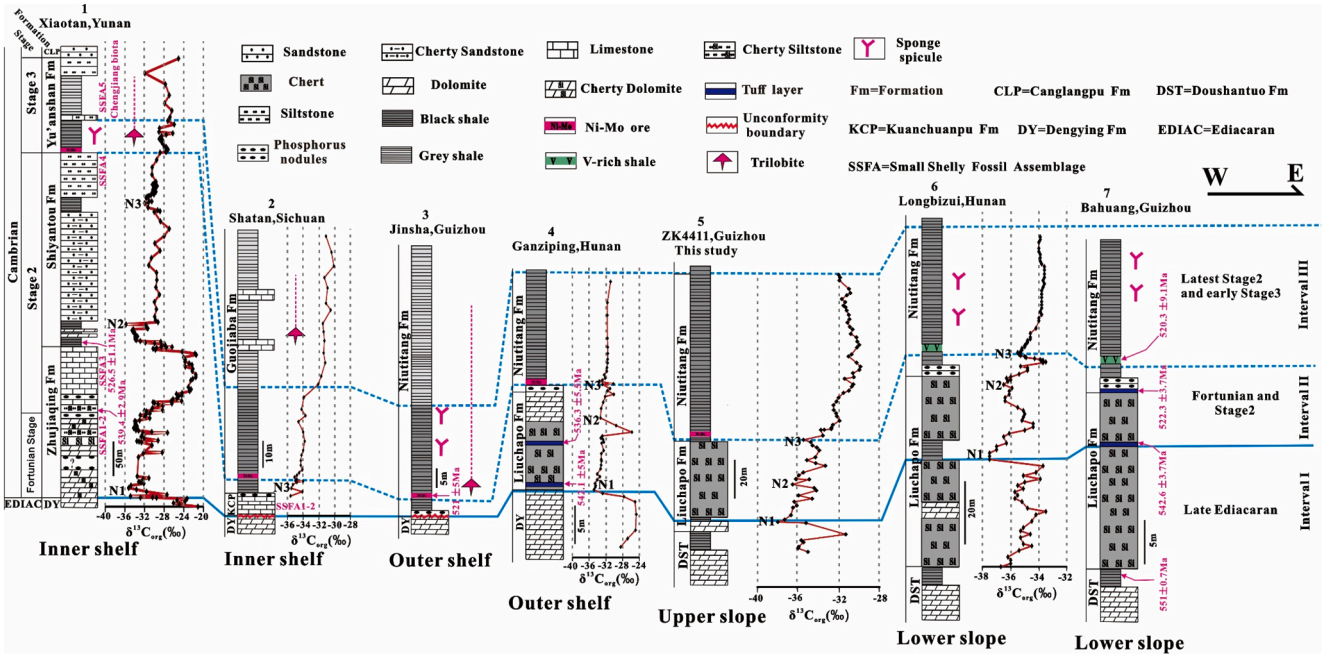

Fig. 2. Stratigraphic correlation across the Yangtze Block from inner shelf to lower slope regions. U–Pb ages for Xiaotan section are from the nearby Meishucun section (Compston et al., 2008; Zhu et al., 2009); Re-Os ages for Ni-Mo ore of Jinsha section and V-rich layer of Bahuang section are from Fu et al. (2016) and Xu et al. (2011); U–Pb ages for Ganziping and Bahuang sections are from Chen et al. (2015a) and Condon et al. (2005). Locations of these typical sections are shown in Fig. 1. 1: Xiaotan section, in Yunnan (Cremonese et al., 2013; Yang et al., 2014; Jin et al., 2016); 2: Shatan section (Goldberg et al., 2007; Guo et al., 2007); 3: Jinsha section (Jin et al., 2016); 4: Ganziping section (Chen et al., 2015a); 5: ZK4411(this study); 6: Longbizui section (Guo et al., 2013); 7: Bahuang section (Chen et al., 2015a).

with a thin layer of polymetallic Ni–Mo sulfide ores (~0.5 m) at the base (Fig. 2).

2.2. Regional stratigraphic correlation

Stratigraphic correlation among the Ediacaran-Cambrian transition sequences in the Yangtze Block is a challenge due to the lack of index fossils at the deep water regions (Wang et al., 2012). The biostratigraphy, U-Pb ages, carbon isotope stratigraphy as well as typical marker layers have been integrated to carry out regional stratigraphy across the Yangtze Block (Wang et al., 2012; Chen et al., 2015a). Based on these correlation tools, three different stratigraphic intervals from I to III are regionally correlated to explore the redox structure and Mo biogeochemistry in the study area.

The Interval I extends from the base of Doushantuo black shales (Member IV) to the E-C boundary (Fig. 2). The organic-rich black shales of Doushantuo (Member IV) can serve as a marker layer, which is well correlated with other equivalent layers in the Yangtze Block, and a precise U-Pb age of 551 ± 0.7 Ma from this marker layer has been reported (Condon et al., 2005; Zhang et al., 2005). However, An et al. (2015) re-investigated the late Ediacaran sedimentary sequences in South China and inferred that the Doushantuo Member IV may have an age older than 551 Ma (likely ≥ 560 Ma). More recently, Rooney et al. (2020) also reported a new estimated age of ~ 565 Ma for the Doushantuo Member IV. A precise U-Pb age of 542 ± 0.3 Ma obtained from Oman has been considered as the boundary between the Cambrian and Ediacaran (Amthor et al., 2003). Linnemann et al. (2019) provided a new radiometric age from a section in Namibia and constrained the Ediacaran–Cambrian boundary to be 538.6–538.8 Ma, over 2 Ma younger than the E-C boundary age reported by Amthor et al. (2003). In South China, the E-C boundary is also defined by the existence of small shelly faunas (SSF) in shallow shelf at the Meishucun/Xiaotan sections and the basal Cambrian negative carbon isotope excursion (BACE) (Zhu et al., 2003, 2006; Chen et al., 2015a). The evident $\delta^{13}C_{org}$ negative excursion of ca. –38‰ (BACE, denoted as N1) in the lower part of the Liuchapo Formation in Well ZK4411 is well correlated with those observed in the base of Zhujiaqing Formation at Xiaotan section in the inner shelf and in the Liuchapo cherts at Ganziping and Longbizui sections in the slope regions (Shen et al., 1998; Chen et al., 2009) (Fig. 2). As a matter of fact, the BACE in South China is also consistent with the frame of the global E-C carbon isotope stratigraphy (Al-Husseini and Ruebsam, 2020 and references therein). These correlations are consistent with the U–Pb ages of 542.1 ± 5.0 Ma and 542.6 ± 3.7 Ma obtained respectively from Ganziping and Bahuang sections, and also supported by the U–Pb ages of 536.7 ± 3.9 Ma obtained from Zhujiaqing Formation at Meishucun section (Zhu et al., 2009) and 536.3 ± 5.5 Ma from the upper Liuchapo Formation at Ganziping section (Chen et al., 2009), considering that the samples for U–Pb dating (Chen et al., 2009; Zhu et al., 2009) are located stratigraphically higher than the E–C boundary.

The Interval II ranges from the E–C boundary upward to the black shales with the third carbon isotope excursion (N3) below the widespread Ni-Mo polymetallic ore and V-rich marker layers and (Fig. 2). The small shelly fossil Assemblage Zones (SSFA) in this interval were restricted in the shelf Xiaotan/Shatan sections and thus its role in the biostratigraphic correlation for the deepwater sections is limited (Wang et al., 2012; Yang et al., 2014). The third negative $\delta^{13}C_{org}$ excursion (N3) is identified around the Ni-Mo sulfide ore and V-rich layers from shallow shelf to slope regions across the whole Yangtze Platform. For example, such a carbon isotope excursion can be traced in the upper part of the Shiyantou Formation at Xiaotan section in Yunnan Province, in the bottom of the Guojiaba Formation black shales at Shatan section in Sichuan Province, and in the basal Niutitang Formation black shales at Ganziping, Longbizui section and Well ZK4411 in Hunan and Guizhou provinces (Fig. 2). Furthermore, the widespread Ni-Mo polymetallic/V-rich marker layers can be well correlated at the base of Yu'anshan Formation in the Xiaotan section (Jin et al., 2016), the base of Guojiaba Formation in the Shatan section (Goldberg et al., 2007), and the base of Niutitang Formation in the Jinsha, Ganziping, ZK4411, Longbizui and Bahuang sections (Guo et al., 2013; Chen et al., 2015a; Jin et al., 2016) (Fig. 2). The Re-Os age of 521 ± 5 Ma (n = 14) obtained from the Ni-Mo sulfide ore layers (Xu et al., 2011) at serval mining sites in the shallow shelf is also consistent with the Re-Os age of 520.3 ± 9.1 Ma obtained from the V-rich layers at Bahuang section (Fu et al., 2016). The two Re-Os ages are also supported by the U–Pb age of 522.3 ± 3.7 Ma from a volcanic ash bed about three meters below the V-rich layer at Bahuang section (Chen et al., 2009), 532.3 ± 0.7 Ma from a volcanic ash bed approximately five meters below the Ni–Mo ore layer at Zhongnancun section (Jiang et al., 2009), and 526.5 ± 1.1 Ma from a tuff layer at the base of the Shiyantou Formation at Meishucun/Xiaotan sections in Yunnan Province (Compston et al., 2008; Zhu et al., 2009).

The Interval III ranges from the top of Interval II upward to the top of the black shale succession (Fig. 2). This interval is characterized by black organic-rich shale successions, which are considered to be formed as a result of large-scale transgression during Cambrian Age 2 and early Age 3 (Cremonese et al., 2013; Feng et al., 2014; Babcock et al., 2015; Wang et al., 2015a). This interval can also be correlated based on (1) the first appearance of trilobites at the shelf Xiaotan /Jinsha sections (Jin et al., 2016) and (2) the similar Sponge spicule fossils in the black shale successions of the shallow shelf Xiaotan/Jinsha sections and deepwater slope Longbizui/Bahuang sections (Chen et al., 2015a; Jin et al., 2016) (Fig. 2). It is worthy to note that although the absence of biostratigraphic fossils and stratigraphic hiatuses in some investigated sections gives rise to some uncertainties regarding the regional stratigraphic correlation, the integration of marker layers, biostratigraphy, radiometric ages and organic carbon isotopes in this study still provides a useful E-C stratigraphic framework in the Yangtze Block.

3. Samples and methods

3.1. Samples

Based on the lithology and thickness of the penetrated strata, forty-two fresh core samples from Well ZK4411 were collected for geochemical analysis, and their depths and lithology are summarized in Table 1. Samples with phosphatic or pyrite nodules were excluded in the present study to avoid any geochemical artefacts. All samples were hand-grounded into a 200 mesh size with agate mortar to avoid any metal contamination.

3.2. Mo isotopic compositions ($\delta^{98/95}$Mo)

The Mo isotope measurements were performed at the State Key Laboratory of Isotope Geochemistry, Guangzhou Institute of Geochemistry, Chinese Academy of Sciences, Guangzhou, China. According to the Mo concentration of each sample, about 6–190 mg of samples were weighed and appropriate amount of ^{97}Mo–^{100}Mo double spikes were added to each sample. Samples were dissolved in 6 ml of a 2:1 mixture of HNO_3 (14 M) and HCl (10 M) at 130 °C. After digestion and drying at 130 °C, the dry residue was then completely re-dissolved in 2–4 ml of a mixture of 0.1 M HF/1 M HNO_3, in preparation for column separation. Mo was separated and purified by ion-exchange chromatography using BPHA resin (Li et al., 2014), and then determined using MC–ICP–MS (Thermo-Fisher Scientific Neptune Plus). The analytical procedures and instrumental parameters for Mo isotope measurements have been detailed in Yin et al. (2018). The Mo isotopic composition was reported as $\delta^{98/95}$Mo relative to reference standard NIST SRM 3134 and calibrated following the procedure of Zhao et al. (2016). Repeated measurements of NIST SRM 3134 standard solutions yielded a mean $\delta^{98/95}$Mo value of 0.00 ± 0.06‰ (2 sd, n = 28). Based on the present analytical conditions, the $\delta^{98/95}$Mo values of IAPSO seawater and SGR-1b oil shale (35 ppm Mo) were measured to be 2.14 ± 0.06‰ and 0.45 ± 0.04‰, respectively, which are consistent with the certified and

Table 1
Total organic carbon (TOC), stable organic carbon isotope ($\delta^{13}C_{org}$), Mo isotope ($\delta^{98/95}Mo$), and selected elemental concentrations and ratios for the ZK4411 core samples.

Sample	Depth (m)	Formation	Lithology	δ^{13}Corg (‰ PDB)	TOC (wt %)	Mo (ppm)	U (ppm)	Mo_{EF}	U_{EF}	$\delta^{98/95}$Mo (‰ NIST3134)	2σ	$\delta^{98/95}Mo_{auth}$ corr.Al	Mn (ppm)	Th/U	Mo/TOC	Re/Mo $\times10^{-3}$	Al (%)
ST-117	652.05	Niutitang	Black shale	−31.95	1.69	45.35	16.02	53.34	6.08	1.06	0.03	1.08	387.40	0.96	26.81	nd	8.50
ST-122	662.15	Niutitang	Black shale	−30.79	2.24	5.75	6.74	7.01	2.65	0.50	0.05	0.52	339.50	2.09	2.57	1.8	8.19
ST-124	665.45	Niutitang	Black shale	−31.65	2.87	43.10	17.48	61.93	8.10	1.33	0.04	1.34	248.50	0.75	15.03	0.69	6.96
ST-18	671.80	Niutitang	Black shale	−31.16	2.70	18.73	9.88	31.39	5.34	0.66	0.04	0.66	87.00	1.11	6.95	0.47	5.97
ST-130	676.65	Niutitang	Black shale	−30.88	0.63	7.29	7.26	46.21	14.84	1.25	0.06	1.27	102.20	0.58	11.57	nd	1.58
ST-132	680.85	Niutitang	Black shale	−30.84	4.11	38.52	17.76	68.81	10.23	1.00	0.03	1.01	121.60	0.68	9.38	0.32	5.60
ST-135	686.65	Niutitang	Black shale	−30.18	3.42	24.30	23.68	46.85	14.73	0.99	0.03	1.01	324.90	0.52	7.10	nd	5.19
ST-138	692.25	Niutitang	Black shale	−30.13	2.37	11.67	11.19	19.52	6.04	0.87	0.04	0.89	352.10	1.02	4.91	nd	5.98
ST-139	696.05	Niutitang	Black shale	−30.67	2.18	9.06	13.47	17.06	8.18	1.15	0.03	1.19	319.00	0.80	4.16	nd	5.31
ST-141	700.65	Niutitang	Black shale	−30.18	4.85	8.01	17.59	14.11	10.00	0.29	0.05	0. 8	646.50	0.66	1.65	0.88	5.68
ST-144	706.45	Niutitang	Black shale	−30.54	2.44	6.33	8.10	7.34	3.03	0.49	0.04	0.50	377.50	1.66	2.60	nd	8.63
ST-146	709.55	Niutitang	Black shale	−31.35	3.84	31.31	7.51	41.56	3.21	0.89	0.04	0.91	742.00	1.79	8.15	0.80	7.53
ST-148	713.85	Niutitang	Black shale	−30.65	0.53	9.22	7.70	11.39	3.07	1.06	0.03	1.12	430.00	1.57	17.48	nd	8.10
ST-149	716.15	Niutitang	Black shale	−30.94	4.44	44.00	24.34	73.95	13.20	1.08	0.04	1.09	843.60	0.51	9.91	0.16	5.95
ST-150	717.35	Niutitang	Black shale	−31.47	6.17	41.02	17.93	81.80	11.53	0.94	0.04	0.95	362.00	0.57	6.65	0.21	5.01
ST-154	726.85	Niutitang	Black shale	–32.44	3.99	78.82	25.67	132.69	13.94	0.81	0.04	0.82	167.40	0.37	19.75	0.04	5.94
ST-157	732.75	Niutitang	Black shale	−31.86	8.18	113.90	61.68	177.36	30.98	1.03	0.04	1.03	268.00	0.18	13.93	0.55	6.42
ST-159	736.55	Niutitang	Black shale	–32.66	7.24	146.70	97.67	82.53	60.68	1.16	0.04	1.16	1313.50	0.11	20.27	0.33	5.19
ST-160	737.35	Niutitang	Mo-rich shale	–32.70	6.27	654.60	63.21	1009.11	31.43	0.73	0.03	0.73	290.80	0.15	104.43	nd	6.49
ST-161	737.75	Niutitang	Ni-Mo ore	–33.38	7.09	1752.80	68.84	2212.88	8.04	0.97	0.05	0.97	156.40	0.20	247.05	nd	7.92
ST-161-1^{REP}		Niutitang	Ni-Mo ore							0.99	0.04						
ST-162	737.85	Niutitang	Black shale	–33.73	4.95	74.50	55.72	136.25	32.87	0.99	0.04	0.99	300.30	0.18	15.04	nd	5.47
ST-163	740.95	Niutitang	Black shale	–33.53	9.74	223.70	74.32	365.67	39.19	−0.07	0.03	−0.07	268.00	0.15	22.96	1.30	6.12
ST-164	743.30	Liuchapo	Black chert	−35.46	7.33	11.88	27.49	493.43	368.32	−0.14	0.03	−0.14	14.10	0.02	1.62	1.15	0.24
ST-164-1^{REP}		Liuchapo	Black chert							−0.15	0.04						
ST-165	744.55	Liuchapo	Black chert	−34.73	7.13	2.82	6.88	37.62	29.63	0.84	0.09	0.85	74.01	0.31	0.39	2.49	0.75
ST-166	746.45	Liuchapo	Black chert	−34.56	1.20	1.90	1.90	59.14	19.15	0.74	0.03	0.75	12.20	0.20	1.58	4.73	0.32
ST-167	747.55	Liuchapo	Black chert	−34.13	0.76	0.77	1.25	20.25	10.59	0.71	0.04	0.72	8.82	0.60	1.02	11.27	0.38
ST-168	749.05	Liuchapo	Black chert	–33.88	1.20	1.71	2.22	17.91	7.53	0.34	0.04	0.34	56.97	1.16	1.42	5.14	0.95
ST-170	752.95	Liuchapo	Black chert	−34.27	1.22	1.30	1.52	4.88	1.85	0.04	0.06	−0.05	27.00	3.27	1.07	10.15	2.66
ST-172	756.25	Liuchapo	Black chert	−34.24	2.41	1.43	1.14	18.15	4.66	0.31	0.04	0.31	51.99	1.53	0.59	10.84	0.79
ST-174	761.35	Liuchapo	Black chert	−35.47	1.51	2.03	3.50	13.89	7.73	0.63	0.04	0.64	12.58	0.69	1.34	5.02	1.46
ST-176	764.95	Liuchapo	Black chert	−36.21	1.94	3.23	3.14	15.92	5.00	0.72	0.23	0.74	18.74	0.66	1.66	4.09	2.03
ST-178	767.95	Liuchapo	Black chert	−36.53	2.24	2.45	4.06	3.60	1.92	0.92	0.04	1.13	66.35	2.29	1.09	0.49	6.81
ST-180	771.35	Liuchapo	Black chert	−34.17	0.13	7.59	5.06	6.98	1.50	0.89	0.04	0.97	179.90	8.31	58.25	nd	10.88
ST-183	777.55	Liuchapo	Black chert	−36.37	2.84	2.80	8.23	3.16	3.00	0.75	0.03	0.92	106.40	1.60	0.99	10.41	8.86
ST-185	780.78	Liuchapo	Black chert	−36.50	2.38	1.20	4.43	2.21	2.63	0.66	0.05	0.87	67.72	1.57	0.51	8.87	5.44
ST-187	787.45	Liuchapo	Black chert	−37.33	0.92	0.64	1.27	0.90	0.58	0.91	0.04		15.19	1.54	0.70	17.29	7.11
ST-188	788.75	Liuchapo	Black shale	−38.01	11.68	4.62	7.46	7.44	3.88	1.05	0.07	1.15	195.70	1.39	0.40	1.15	6.20
ST-188-1^{REP}		Liuchapo	Black shale							1.05	0.07						
ST-192	795.55	Doushantuo	Black shale	−31.25	8.38	74.63	36.87	171.80	27.38	1.02	0.04	1.03	152.00	0.34	8.90	0.33	4.34
ST-192-1^{REP}		Doushantuo	Black shale							0.98	0.04						
ST-193	798.85	Doushantuo	Black shale	−35.68	1.68	17.74	19.68	385.10	137.81	0.89	0.08	0.89	2764.10	0.09	10.54	0.47	0.46
ST-194	799.95	Doushantuo	Black shale	−35.45	5.04	82.41	10.05	134.39	5.29	0.33	0.03	0.33	87.50	1.67	16.34	2.89	6.13
ST-194-1^{REP}		Doushantuo	Black shale							0.22	0.05						
ST-195	802.45	Doushantuo	Black shale	−35.93	3.65	91.64	16.92	148.61	8.85	−0.60	0.03	−0.60	234.90	1.01	25.13	2.24	6.17
ST-196	803.25	Doushantuo	Black shale	−35.99	3.84	63.51	18.13	94.32	8.69	−0.47	0.03	−0.48	135.50	0.97	16.54	4.31	6.73

REP = Repeat; nd = Not determined.

Note: the corrected $\delta^{98/95}Mo$ values were calculated following the formula: $\delta^{98/95}Mo_{auth} = [(\delta^{98/95}Mo_{tot} \times Mo_{tot}\text{-}\delta^{98/95}Mo_{det} \times Mo_{det})/Mo_{auth}]$ (Poulson Brucker et al., 2009; Wen et al., 2015), in which the detrital Mo concentration (Mo_{det}) was given by $Mo_{det} = [(Mo/Al)_{PAAS} \times Al_{tot}]$ and the authigenic Mo concentration was calculated by $Mo_{auth} = Mo_{tot}\text{-}Mo_{det}$. Mo and Al concentration of PAAS (1.0 ppm, 10%, respectively) (Taylor and McLennan, 1985) and $\delta^{98/95}Mo_{det}$ value of 0.4‰ (Dahl et al., 2011) were used for detritus correction.

early reported values (Zhao et al, 2016; Yin et al., 2018). The Mo procedural blank was<0.1 ng, thus can be ignored compared with the Mo concentrations of our samples. Nägler et al. (2014) suggested that setting the $\delta^{98/95}$Mo value of NIST SRM 3134 to be +0.25‰ will facilitate the use of canonical values, such as +2.3‰ for seawater and –0.7‰ for marine Fe–Mn precipitates. Therefore, the $\delta^{98/95}$Mo values relative to NIST SRM 3134 (+0.25‰) can be recalculated as follows (Eq. (1)):

$$\delta^{98/95}\mathrm{Mo}(‰) = \left(\frac{\left(^{98/95}\mathrm{Mo}\right)_{\mathrm{sample}}}{\left(^{98/95}\mathrm{Mo}\right)_{\mathrm{NIST3134}} * 0.99975} - 1 \right) * 1000 \quad (1)$$

3.3. TOC and organic carbon isotopic ($\delta^{13}C_{org}$)

An approximate amount of each sample (80–150 mg) was weighed and treated with diluted hydrochloric acid (HCl, 6 mol/L) to thoroughly remove carbonates; hence the remains were washed and centrifuged with Milli-Q water to remove chlorides and dried at 60 °C overnight before instrumental analysis. Measurements of total organic carbon content (TOC) were conducted on a Leco CS230 carbon/sulfur analyzer.

The measurements of organic carbon isotopic composition were carried out on carbonate-free samples using Delta XL Plus isotope mass spectrometer. The results were reported in delta notation ($\delta^{13}C_{org}$) relative to the Vienna Peedee Belemnite (VPDB) in per mil and the reproducibility of replicate analyses was better than ± 0.3‰.

3.4. Major, trace and rare earth elements

Major oxides of powdered samples were determined using a ZSX 100e X-ray fluorescence spectrometry (XRF) on fusion glasses with a 1:10 ratio of sample to $Li_2B_4O_7$ flux. The analytical precision of XRF was better than 5%. Concentrations of trace and rare earth elements were measured on a Thermo Scientific Element XR inductively coupled plasma mass spectrometry (ICP-MS) after sample powders were digested sequentially with HNO_3 (8 M), $HClO_4$ (3 M) and HF (21 M) in high-pressure Teflon cups. The analytical precision was better than 7% for trace elements and 10% for rare earth elements.

Element enrichment factors (EFs) were calculated according to $X_{EF} = [(X/Al)_{sample}/(X/Al)_{PAAS}]$, where X and Al represent weight percent of elements X and Al, and the subscripts of sample and PAAS denote the sample under study and the Post-Archean Australian Shale (PAAS) standard (Taylor and McLennan, 1985), respectively.

4. Results

Concentrations of TOC, trace and rare earth elements as well as $\delta^{98/95}$Mo and $\delta^{13}C_{org}$ values for all the samples are summarized in Table 1.

The TOC values of Interval I (788.8–803.3 m) vary from 1.7 to 8.4 wt % with an average of 4.5 wt%, and the $\delta^{13}C_{org}$ values in this interval fluctuate between −35.9‰ and −31.2‰. Mo concentrations are relatively high, fluctuating between 17.7 ppm and 91.6 ppm with an average of 65.9 ppm, and the $\delta^{98/95}$Mo values show an increasing upward shift from –0.6‰ to +1.02‰ (Fig. 3). Relatively high Mo/TOC ratios (8.9–25), low Th/U ratios (0.1–1.7) and low Re/Mo ratios (0.3–4.3) are observed in this interval, and the concentrations of Mn vary between 136 ppm and 2764 ppm with an average of 715 ppm (Fig. 3).

For the Interval II (743.3–788.8 m), the $\delta^{13}C_{org}$ values vary between −38.0‰ and −33.8‰ and exhibit an upward positive shift though slightly fluctuated (Fig. 3). The TOC values reach the maximum of 11.7 wt% corresponding to the minimum $\delta^{13}C_{org}$ value of −38.0‰ at the boundary between Interval I and Interval II (788.8 m), and then start to decrease rapidly to 0.1–7.3 wt%, with an average value of 2.4 wt%. The $\delta^{98/95}$Mo values show a general upward decreasing trend from +1.05‰ to –0.14‰, and the Mo concentrations vary between 0.6 ppm and 11.9 ppm with an average value of 3.1 ppm, slightly higher than Mo concentration (1.0 ppm) of PAAS. Similarly, except one anomaly, Mo/TOC ratios (0.4–1.7) and Mn concentrations (14.1–106.4 ppm) are low relative to those of Interval I. The Th/U ratios fluctuate between 0.01 and 8.3 with an average of 1.7. The Re/Mo ratios of this interval are obviously higher than those of Interval I and range from 0.5 to 17.3 (Fig. 3).

As shown in Fig. 3, there are abrupt changes across the boundary between Interval II and Interval III (743.3 m) in many geochemical parameters, including the TOC, Mo, U, and Mn contents, $\delta^{13}C_{org}$ and $\delta^{98/95}$Mo values, Mo/TOC ratios and Re/Mo ratios. In the Interval III (652.1–743.3 m), the $\delta^{13}C_{org}$ values show an upward positive shift from −35.5‰ at the boundary between Interval II and Interval III (743.3 m) to −30.1‰ in the middle part (686.7–700.7 m), and then gradually decrease to −31.9‰ at the top (652.1 m). The TOC values display a steady upward decrease and vary between 0.6 and 8.2 wt% (avg. 3.9 wt %). The Mo concentrations of two samples in the Ni-Mo polymetallic ore layers (737.4–737.8 m) are 1715 and 656 ppm, respectively, which correspond to Mo/TOC ratios of 247 and 104; other samples in this interval have Mo concentrations fluctuating between 5.7 ppm and 223.7 ppm (avg. 49.1 ppm) and display Mo/TOC ratios in the range of 1.7–26.8 (avg. 10.5). At the base part of Interval III (743.3 m), there is a sudden upward increase in $\delta^{98/95}$Mo values from –0.14‰ to 0.99‰, and then they fluctuate between 0.29 and 1.33‰. Compared with the Interval II, the Th/U ratios in the Interval III decrease to 0.11–2.1 with an average of 0.75, and a rapid decrease of Re/Mo ratios (from 1.3 to 0.3) in

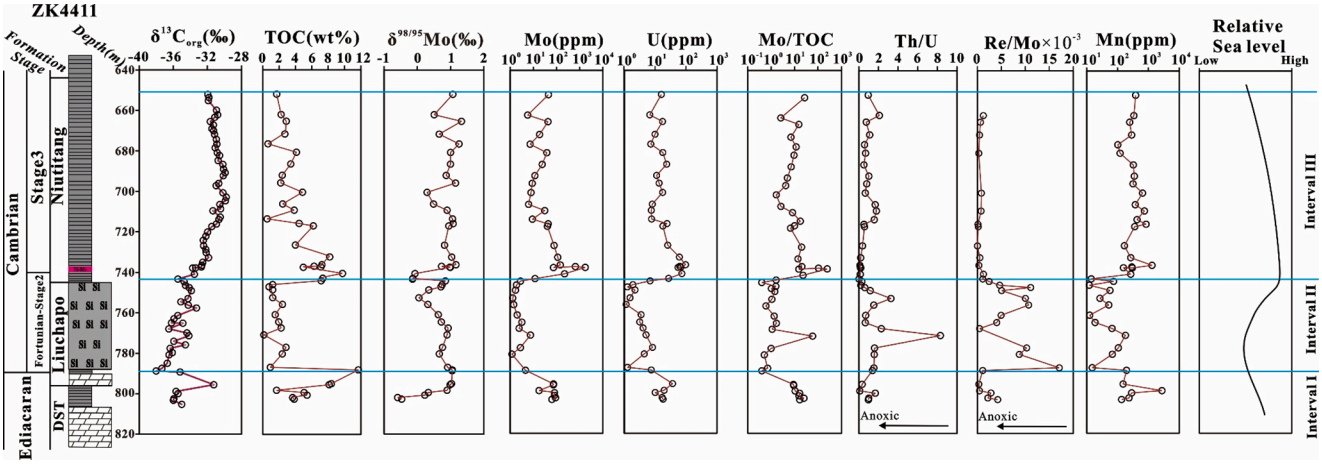

Fig. 3. Profiles of TOC, Mo, Mn concentrations, organic carbon and Mo isotopes, Mo/TOC, Th/U and Re/Mo ratios. The curve of sea level change during the E-C transition is from Babcock et al. (2015).

this interval was also recognized (Fig. 3).

5. Discussion

5.1. Evolution of marine redox conditions

Geochemical redox proxies, including concentrations of redox-sensitive trace elements and their ratios, Mo-U covariation patterns, and Fe speciation data have been widely used as indicators of paleo-redox conditions (Hatch and Leventhal, 1992; Jones and Manning, 1994; Algeo and Maynard, 2004; Tribovillard et al., 2006; Canfield et al., 2008; Algeo and Tribovillard, 2009; Algeo and Li, 2020). Recently, some authors suggest that the absolute values of trace metal ratios have to be treated qualitatively and it is their changes with depth that should be used to discuss the paleo-environmental variation (Ruebsam et al., 2017; Algeo and Li, 2020; Liu and Algeo, 2020). Therefore, changes of trace metal ratios with depth rather than their thresholds are qualitatively used to trace redox variation in this study. Some trace elements (Mo, U, V) are sensitive to redox conditions and become enriched in sediments under anoxic bottom water condition (Crusius and Thomson, 2000; Algeo and Maynard, 2004). For example, Thorium has one redox state (Th^{4+}) and is quickly removed from the water column via adsorption on detrital material, in particular clay minerals, iron, aluminum, and manganese oxides, and organic matter. In contrast, uranium has two redox states (U^{4+} and U^{6+}). Under reducing conditions, U^{4+} is insoluble and thus can be fixed and further supplied by diffusion from seawater, resulting in low Th/U ratios (Jones and Manning, 1994). Therefore, sedimentary Th/U ratio can act as a redox indicator and lower Th/U ratios indicate more reducing water condition (Wignall and Twitchett, 1996). Based on studies of different modern marine systems, the Mo_{EF}-U_{EF} covariation patterns are proved to have the ability to identify redox conditions and the Fe-Mn particulate shuttles (Algeo and Tribovillard, 2009; Tribovillard et al., 2012).

Rhenium accumulation in sediments depends mainly on the degree of reducing conditions (Turgeon and Brumsack, 2006). The behavior of molybdenum is somewhat similar to Re, and Mo can be efficiently transferred into sediments under euxinic waters containing high H_2S concentrations (Turgeon and Brumsack, 2006). The sedimentary Re/Mo ratios can also be used to distinguish between anoxic and suboxic water conditions, and low Re/Mo ratios indicate an anoxic water condition, while high Re/Mo ratios represent less reducing water conditions (Crusius et al, 1996; Turgeon and Brumsack, 2006). Based on these geochemical proxies, redox conditions for the three intervals (I, II and III) during the E-C transition are discussed below.

5.1.1. Interval I: Widespread euxinic condition during the late Ediacaran

As a regional marker layer, the widespread organic-rich black shales in the member IV of the Doushantuo Formation were formed under widespread anoxic/euxinic water conditions (Kendall et al., 2015; Zhai et al., 2018; Fang et al., 2019). In this study, high Mo and U concentrations (avg. 66 and 20 ppm, respectively), low Th/U ratios (avg. 1.4) observed in this interval also indicate anoxic water conditions in the upper slope setting. Three samples yield low Re/Mo ratios (avg. 3.2×10^{-3}), indicating anoxic water condition; while the lower Re/Mo ratios of two samples (avg. 0.4×10^{-3}) may point to more reducing condition. This interpretation is further evidenced in the diagram of Mo_{EF}-U_{EF} covariation where most samples plot in the field of anoxic/euxinic conditions (Fig. 4). In the Gorges/Rongxi/Wuhe sections, iron specitions data ($Fe_{HR}/Fe_T > 0.38$; $Fe_{py}/Fe_{HR} > 0.7$) also attest to widespread euxinic conditions from the shallow shelf to the deep water slope (Kendall et al., 2015; Sahoo, 2015; Sahoo et al., 2016). Some studies suggest a 'sandwich'-like model for the Ediacaran ocean where the mid-depth euxinic water was sandwiched between oxic surface water and ferruginous deep water (Li et al., 2010, 2012; Poulton et al., 2010; Reinhard et al., 2009). The present study further reveals that during the deposition of Interval I, the mid-depth euxinic water conditions may spread over the Yangtze Platform, whereas the oxic water conditions may be limited to the shallow surface waters.

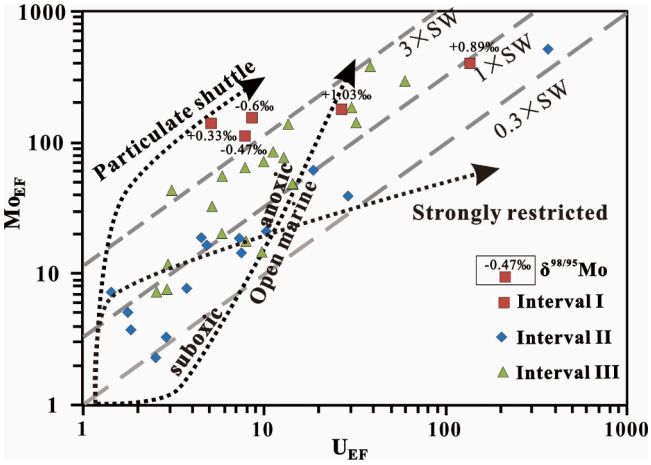

Fig. 4. Plot of Mo_{EF} versus U_{EF} for the ZK4411 core samples. The gray dashed lines represent different Mo:U ratios of modern seawater (0.3, 1, and 3). The black dotted trend line represents the"open marine" trend from suboxic to euxinic regions, the "particulate shuttle" trend, and the "restricted" trend, respectively. Modified from Algeo and Tribovillard (2009).

5.1.2. Interval II: Anoxic with occasional suboxic conditions during Cambrian Fortunian and Stage 2

After the deposition of Doushantuo organic-rich black shales, the sea level began to fall at the end of the Ediacaran, and the Dengying dolomites in the shallow shelf and the Liuchapo cherts in the deepwater slope and basin regions were formed (Jiang et al., 2011; Zhai et al., 2018). A major sea level lowstand is also predicted for the latest Ediacaran in the Sukharikha section in Russia, which occurs just below the BACE (Al-Husseini and Ruebsam, 2020). It is worthy to note that the low concentrations of Mo and U (avg. 2.4 and 3.7 ppm, respectively) in this interval may be ascribed to the severe Mo depletion in strongly restricted basins and therefore could not be effectively used to trace redox conditions (Algeo and Lyons, 2006). In this interval, most samples exhibit relatively high Re/Mo ratios (from 1.2×10^{-3} to 17.3×10^{-3}) (Fig. 3), indicating dominant anoxic with occasional suboxic water conditions. Except for two samples, most samples have low Th/U ratios, also suggesting the dominance of anoxic waters. In the Mo_{EF}-U_{EF} diagram, samples plot in the field for suboxic-anoxic conditions, further supporting this interpretation (Fig. 4). In addition, the ratios of $Fe_{HR}/Fe_T > 0.38$ observed in the contemporaneous Liuchapo cherts at lower slope Longbizui/Xugongping sections also suggest ferruginous deep-water conditions (Wang et al., 2012; Chang et al., 2018). Some researchers considered that the stratified ocean redox structure may also continue to exist during the earliest Cambrian (Feng et al., 2014; Jin et al., 2016). In general, the stratified ocean with oxic surface waters in the shallow shelf and anoxic ferruginous deep waters in the slope and basin regions prevailed in this interval (Fan et al., 2016; Zhai et al., 2018), and the oxic surface waters may sometimes spread to the mid-depth upper slope region.

5.1.3. Interval III: Anoxic with intermittent euxinic water during early Cambrian Stage 3

In this interval, the organic-rich black shales were widely formed from shallow shelf to deep water slope and basin regions across the whole Yangtze Platform due to large-scale transgression (Goldberg et al., 2007; Pi et al., 2013; Feng et al., 2014; Babcock et al., 2015). Samples from this interval show high Mo concentrations (avg. 154 ppm) and low Th/U ratios (avg. 0.75), indicating anoxic bottom water conditions. The Re/Mo ratios (avg. 0.6), close to the value of the present-day seawater (0.8×10^{-3}, Crusius et al. (1996)), indicate more reducing anoxic water

condition. This interpretation is also supported by the diagram of Mo_{EF}-U_{EF}, in which most samples are plotted in the anoxic region (Fig. 4). It is worthy to note that the regional Ni-Mo sulfide ore layer with extreme high concentrations of Mo (1753 ppm) at the base of Interval III may indicate temporarily euxinic water condition with high H_2S concentration in the column during the latest Age 2. Early studies of this widespread ore layer also proposed persistently euxinic water conditions and H_2S-rich bottom waters based on iron speciation data, Mo and sulfur isotopic data (Jiang et al., 2007; Lehmann et al., 2007; Wille et al., 2008; Xu et al., 2013; Gao et al., 2018). All these facts indicate that dominantly anoxic with intermittently euxinic water conditions prevailed in this interval in the upper slope region, which is also consistent with the widespread anoxic/euxinic water conditions across the Yangtze Block during the Cambrian Age 2 and early Age 3 (Jin et al., 2016).

5.2. Restricted basin during the earliest Cambrian

The global paleogeographic reconstructions indicated the region of the present South China, consisting of the Yangtze and Cathaysia blocks, was an isolated craton surrounded by the open ocean during the E-C transition (Li et al., 2008). The connectivity between the Yangtze and Cathaysia blocks is still uncertain, and the influence of Cathaysia Block on the restriction of the Yangtze paleo-ocean is also under debate (Li et al., 2009). The worldwide small shelly fossils (SSFs) and the globally correlated carbonate carbon isotope profiles on the Yangtze Platform seem to suggest a good connection with open ocean (Zhu et al., 2003; Steiner et al., 2007; Chen et al., 2015a; Xiang et al., 2017; Al-Husseini and Ruebsam, 2020). However, some studies proposed that the Yangtze platform evolved into restricted basin and was separated from open ocean by uplifts during the E-C transition (Steiner et al., 2001; Goldberg et al., 2007; Xu et al., 2013; Yeasmin et al., 2017). Molybdenum (Mo) is redox sensitive and can be rapidly transferred from water column into sediments under euxinic conditions (Tribovillard et al., 2006). For restricted basins, aqueous Mo will become depleted through sink to sediments when adequate resupply from open ocean is limited, thus subsequently resulting in reduced Mo concentrations in later sediments (Algeo and Lyons, 2006). In this study, obviously low Mo concentrations (avg. 3.1 ppm) were observed in the Interval II that was formed under dominantly anoxic water conditions. Similarly, low Mo concentrations (avg. 4 ppm) were also reported in the stratigraphic equivalent Liuchapo cherts at Xugongping/Longbizui sections, which were also deposited under anoxic ferruginous deepwater conditions (Och et al., 2016; Chang et al., 2018). Thus, the low Mo concentrations of this interval is most likely ascribed to the strong restriction of water column and the limited supply of aqueous Mo from open ocean.

Although the Mo concentration in this interval may be diluted by the high abundance of Si in the Liuchapo cherts, the dilution effects on elemental ratios are expected to be minor, and thus these geochemical ratios determined for the cherts can be effectively used to trace paleo-environmental variations (Chen et al., 2009; Wang et al., 2012; Chang et al., 2018). The degree of basin restriction could be effectively distinguished by sedimentary Mo/TOC ratios (Algeo and Lyons, 2006). Based on detailed studies of different modern silled marine basins, the range of sediment Mo/TOC (ppm/wt.%) ratios are 4.5 for the Black Sea, 9–25 for Framvaren Fjord and Cariaco basin, and 45 for Saanich Inlet, representing strong, moderate and weak restriction, respectively (Algeo and Lyons, 2006; Algeo and Rowe, 2012). However, the Mo concentrations of early Cambrian ocean (ca. 50 nmol) (Wang et al., 2015b) were lower than that of modern seawater (ca. 105 nmol), which may influence the judgement of water restriction during early Cambrian (Algeo and Maynard, 2004; Cheng et al., 2016). According to statistical Mo/TOC ratios of early Cambrian black shales, Cheng et al. (2016) reported a mean Mo/TOC value of 11 (n = 238), and proposed early Cambrian oceanic sediments with Mo/TOC ratios higher than 11 ppm/wt.% were considered as good connectivity with the open ocean. In this study, samples of the Intervals I and III show relatively high Mo/TOC ratios (avg. 15.5 and 26.3, respectively), indicating a good connectivity with the open ocean. However, except one sample with low TOC (<0.5 wt%), all the other samples of Interval II have low Mo/TOC ratios (avg. 1.1 ppm/wt.%), which are even smaller than the value of 4.5 ppm/wt.% for the strongly restricted modern Black Sea (Algeo and Lyons, 2006). These results indicate a strongly restricted basin with reduced water exchange with the open ocean (Fig. 5). This inference is also supported by similar low Mo/TOC ratios (avg. 3.2) of the same Liuchapo cherts at Xugongping/Longbizui sections (Och et al., 2016; Chang et al., 2018) (Fig. 5).

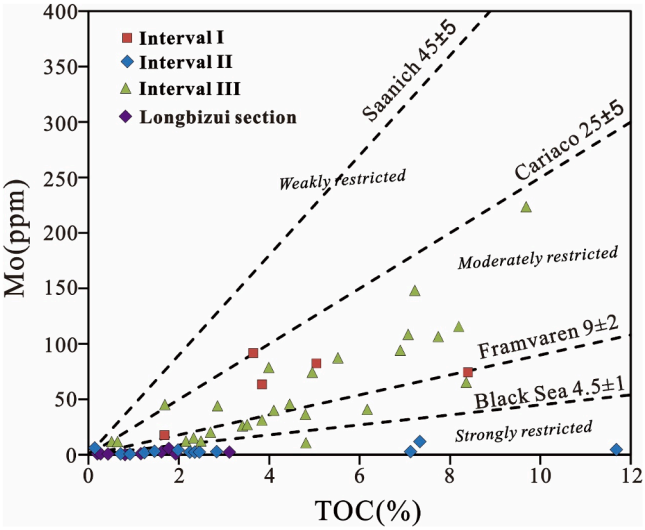

Fig. 5. Cross plot of Mo concentration versus TOC for the ZK4411 core samples. The Mo and TOC contents of Longbizui section cherts are from Och et al. (2016). Dashed lines represent the regression trends for the four modern anoxic marine systems (Saanich Inlet, Cariaco Basin, Framvaren Fjord, and Black sea), showing variable degrees of hydrographic restriction (Algeo and Lyons, 2006).

Overall, we consider that the Yangtze platform was well connected with open ocean during the deposition time of Interval I (late Ediacaran), and then became strongly restricted during the deposition time of Interval II (Cambrian Fortunian and Age 2). The Liuchapo cherts were likely formed in the restricted silica-rich basin where trace metal concentrations in seawater are low due to limited supply from open ocean (Chang et al., 2018). Afterwards, a large-scale transgression during Cambrian Age 2 enhanced the connectivity with the open ocean and oxic waters plus nutrients and trace metals flowed into restricted basin, as shown by the abrupt increase of TOC, Mo and U concentrations, Mo/TOC ratios at the boundary between interval II and interval III in Fig. 3.

5.3. Interpretation of Mo isotope variations during E-C transition

Brucker et al. (2009) suggested that the sedimentary Mo isotopic compositions may be influenced by lithogenic Mo into bulk sediments through continental weathering. Therefore, it is necessary to constrain the isotopic composition of sedimentary authigenic Mo ($\delta^{98/95}Mo_{auth}$) and the measured Mo isotope compositions ($\delta^{98/95}Mo$) of bulk rocks require correction for dilution by the detrital contribution ($\delta^{98/95}Mo_{det}$). To eliminate the detrital contribution, all the measured $\delta^{98/95}Mo$ values on our bulk shale samples were recalculated according to their Al concentrations following the formula proposed by Brucker et al. (2009) and Wen et al. (2015). For most samples in this study, the measured ($\delta^{98/95}Mo$) and corrected values ($\delta^{98/95}Mo_{auth}$) are nearly equivalent (Table 1), indicating minor detrital Mo effects on bulk Mo isotopes. And therefore the following discussion is based on the measured $\delta^{98/95}Mo$ values.

5.3.1. Interval I : Mn particulate shuttles in the stratified late Ediacaran ocean

In this interval, redox sensitive elements and iron speciation data from this study site and adjacent shelf/slope areas indicate the ocean was stratified with oxic surface waters and anoxic/euxinic deep waters (Sahoo et al., 2016; Fang et al., 2019), which is consistent with the stratified Ediacaran Ocean model proposed by Li et al. (2010). The $\delta^{98/95}$Mo values show a positive shift from –0.6‰ at the bottom to +1.02‰ at the top, and similar shifts were also observed at Three Gorges section (from –0.27‰ to +2.08‰) (Kendall et al., 2015), Rongxi and Wuhe sections (from –1.37‰ to +1.32‰) (Ostrander et al., 2019) (Fig. 6). Considering that it is impossible for the seawater $\delta^{98/95}$Mo value to be lower than the mean $\delta^{98/95}$Mo value of riverine inputs (ca. +0.7‰) (Archer and Vance, 2008), the negative $\delta^{98/95}$Mo values (<0‰) in the lower part of this interval cannot reflect the $\delta^{98/95}$Mo value of seawater at the time, and such negative $\delta^{98/95}$Mo values in the sediments are most likely related to significant Mo isotopic fractionation.

One possible mechanism for such a large Mo isotope fractionation is the shuttling of isotopically light Mo to euxinic sediments by Mn oxides (Scholz et al., 2013; Cheng et al., 2016; Ostrander et al., 2019). Mn particulate shuttles have been found in stratified modern oceans such as the Baltic Sea where they can efficiently transfer Mo to euxinic water column and sediments due to the presence of redox gradient at the chemoclines of fluctuating O_2/H_2S (Dellwig et al., 2010; Scholz et al., 2013). The negative $\delta^{98/95}$Mo values may also reflect delivery of lighter Mo isotopes to sediments by Mn particulate shuttles in the stratified late Ediacaran ocean, which is different from the preferential adsorption of isotopically light Mo by Mn oxides under oxic waters (Barling et al., 2001).

For our samples, the existence of Mn particulate shuttles is supported by the Mo_{EF}-U_{EF} enrichment pattern (Fig. 4), in which the samples with negative $\delta^{98/95}$Mo values yield high Mo/U ratios (3 times higher than that of modern seawater) near to Mn particulate shuttle, similar to that observed in the modern weakly euxinic Cariaco Basin (Algeo and Tribovillard, 2009). The Mn oxyhydroxide particles preferentially adsorb isotopically light Mo above the chemocline and then sink into the euxinic water column. Under the absence of oxygen, Mn oxides are mobilized during the process of reductive dissolution (from Mn^{4+} to Mn^{2+}) (Calvert and Pedersen, 1996; Morford et al., 2009) and isotopically-light Mo is released to euxinic waters (Fig. 7a). Subsequently, Mo is precipitated from the water column and gets enriched in the sediment (Tribovillard, 2006; Scholz et al., 2011). This process is also consistent with the deficit of Mn (avg. 219 ppm) in this interval relative to that of PAAS (850 ppm) because of reductive dissolution without supporting Mn accumulation in marine sediments and relatively high Mo concentration (avg. 79 ppm). Shuttling of isotopically light Mo to euxinic sediments by Mn oxides results in negative sedimentary $\delta^{98/95}$Mo values, which can be nearly 3.0‰ lighter than the contemporaneous seawater, just like the cases in the modern Baltic Sea and Cariaco Basin (Arnold et al., 2004; Scholz et al., 2013).

Alternatively, the incomplete conversion of molybdate (MoO_4^{2-}) under weakly euxinic water conditions (e.g., $[H_2S]_{aq} < 11$ μM) may also cause large Mo isotope fractionation (Arnold et al., 2004; Neubert et al., 2008; Nägler et al., 2011). The ratios of $Fe_{HR}/Fe_T > 0.38$ and $Fe_{py}/Fe_{HR} > 0.7$ reflect euxinic waters in this interval (Fig. 6), and thus the negative $\delta^{98/95}$Mo values may also be ascribed to Mo isotope fractionation under weakly euxinic water condition (e.g., $[H_2S]_{aq} < 11$ μM), which can be up to 3.0‰ lighter than seawater $\delta^{98/95}$Mo value in the Black Sea (Nägler et al., 2011). In summary, the negative $\delta^{98/95}$Mo values observed in the lower part of this interval are mainly ascribe to deliver

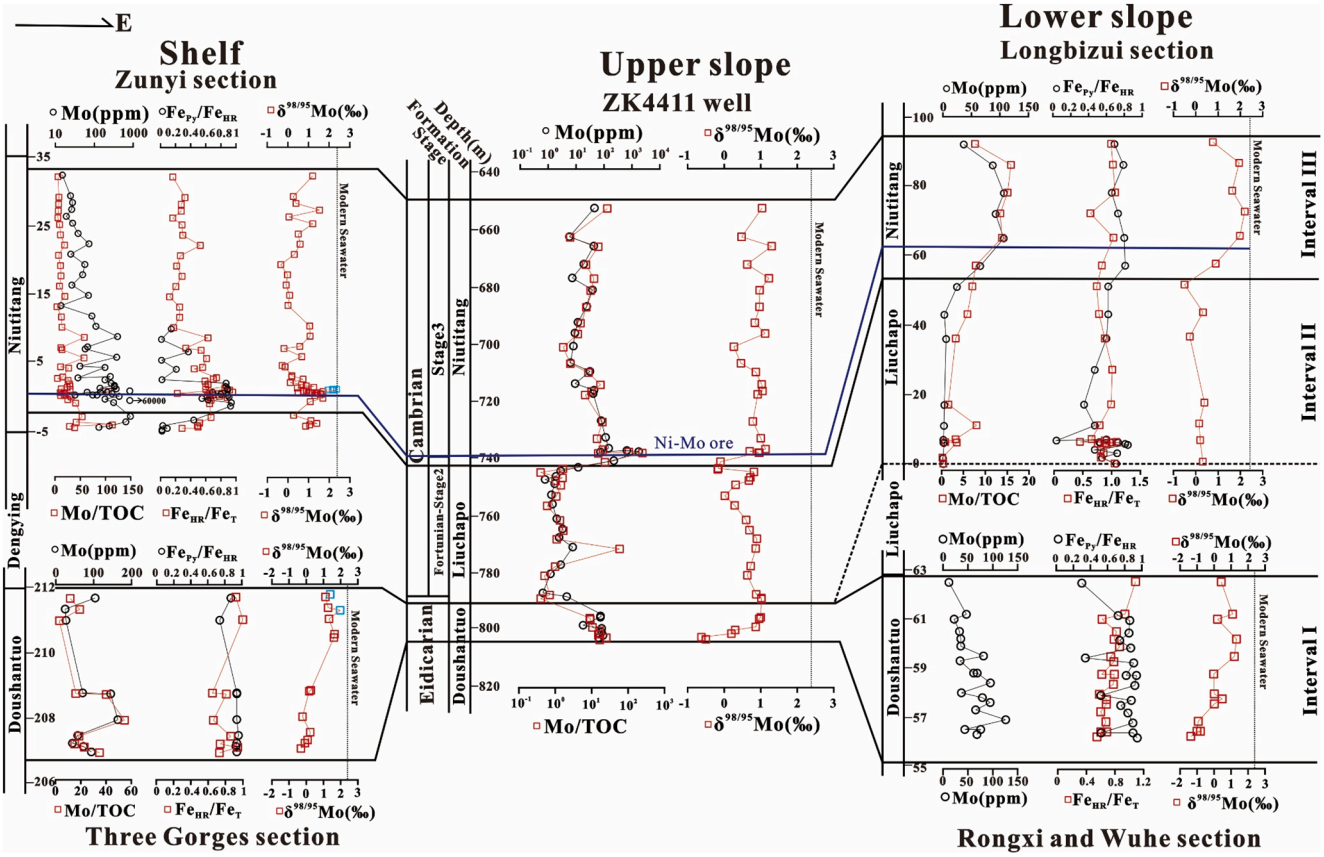

Fig. 6. Correlated profiles of Mo concentration, Mo/TOC ratios, iron speciation data, and $\delta^{98/95}$Mo values from shelf to slope regions. The Zunyi section is from Xu et al. (2012) and Wen et al. (2015); the Three Gorges section is from Kendall et al. (2015); the Longbizui section is from Chen et al. (2015b); the Rongxi and Wuhe sections are from Sahoo (2015), Sahoo et al. (2016) and Ostrander et al. (2019).

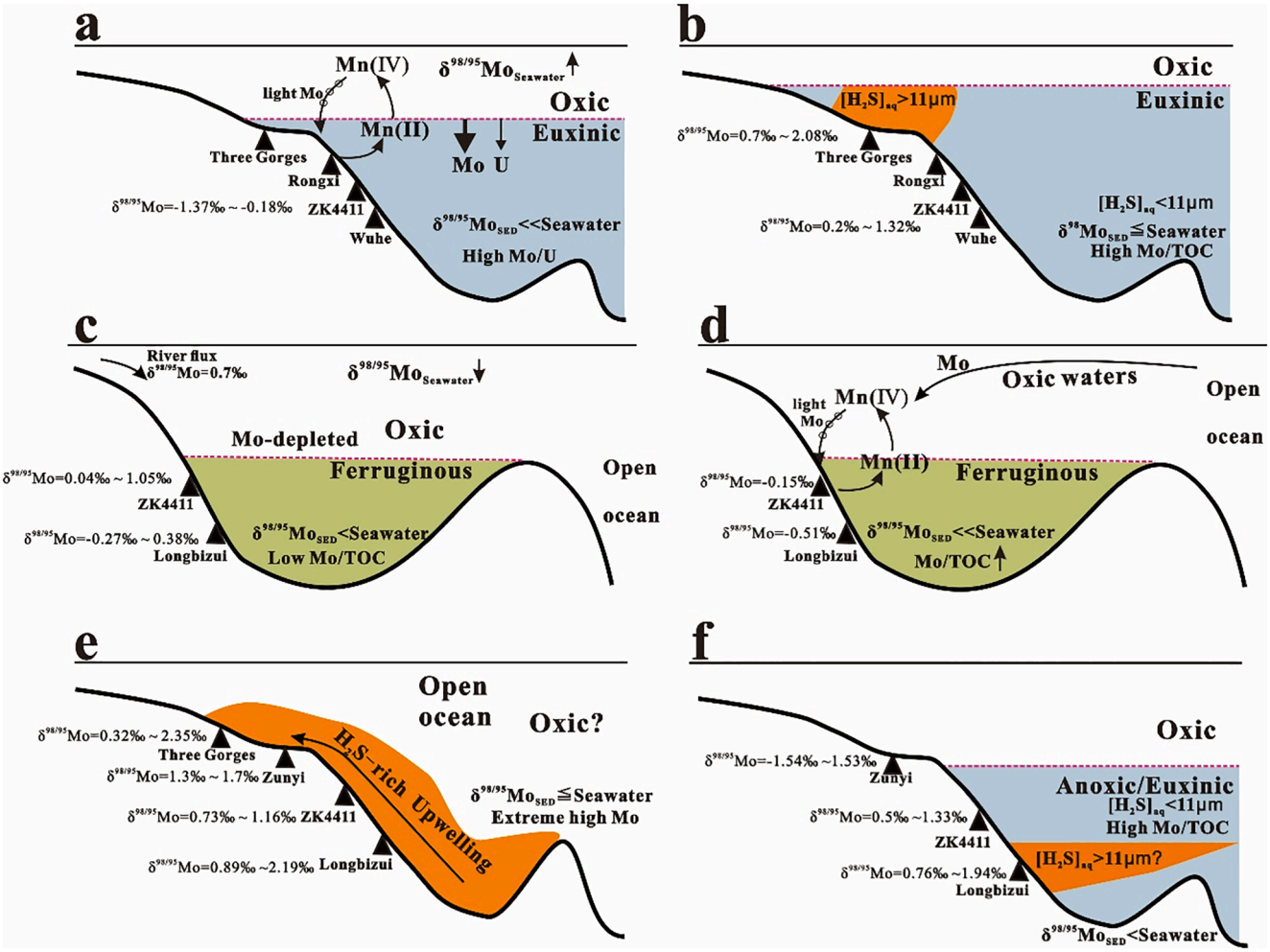

Fig. 7. Schematic evolutional pattern of redox structure and Mo biogeochemistry across the E-C transition. a: the lower part of Interval I (late Ediacaran); b: the upper part of Interval I (late Ediacaran); c: the Interval II (Cambrian Fortunian and Age 2); d: the uppermost part of Interval II (late Age 2); e: the lowermost part of Interval III (latest Age 2); f: the Interval III (early Age 3).

isotopically light Mo to euxinic sediments by Mn oxides shuttles, or the low H_2S concentration in euxinic waters with a large Mo isotopes fractionation, or probably both.

By contrast, relatively high $\delta^{98/95}$Mo values (0.2–2.08‰) can be clearly identified in the upper part of this interval at Well ZK4411 and Three Gorges /Rongxi /Wuhe sections (Fig. 6). In the diagram of Mo_{EF}-U_{EF} (Fig. 4), these samples yield moderate Mo/U ratios between 1 and 3 times of those of modern seawater, indicating anoxic waters of open ocean without Mn particulate shuttles. The wide range of $\delta^{98/95}$Mo values may be attributed to incomplete conversion of molybdate with large Mo isotopic fractionation under weakly euxinic condition (e.g., $[H_2S]aq < 11$ μM) (Helz et al., 1996; Arnold et al., 2004).

5.3.2. *Interval II : Mo isotope variations in the restricted basin*

As discussed in section 5.2, the Yangtze Block became a strongly restricted basin during Interval II (the earliest Cambrian), with a stratified water column and oxic surface water overlaying anoxic ferruginous deep water. The relatively low $\delta^{98/95}$Mo values (0.04–1.05‰) were observed in this interval, and similar lower $\delta^{98/95}$Mo values (–0.27 to +0.38‰) were also be recognized at Longbizui section (Chen et al., 2015b) (Fig. 6). Some $\delta^{98/95}$Mo values below 0.7‰ may indicate Mo isotope fractionation from coeval seawater due to incomplete conversion of molybdate (MoO_4^{2-}) under anoxic ferruginous waters. It is worthy to note that Mo isotopic composition of coeval seawater may decrease in a restricted basin without free exchange with open ocean (Xu et al., 2012, 2013). This is mainly caused by the depletion of aqueous Mo in restricted seawater due to limited resupply from open ocean and the Mo influx is dominated by continental input. In this situation, the $\delta^{98/95}$Mo values of seawater may decrease toward the continental input Mo isotope signature (ca. +0.7‰) until there is replenishment by the open ocean with heavy Mo isotope (Xu et al., 2012). Similar observations were also reported for the Permian black shales from Europe (Ruebsam et al., 2017). Therefore, the relatively low $\delta^{98/95}$Mo values in this interval may reflect Mo isotope fractionation under anoxic ferruginous waters, or the decrease of $\delta^{98/95}Mo_{Seawater}$ values in the restricted basin (Fig. 7c).

It is worthy to note that negative $\delta^{98/95}$Mo excursions (–0.15‰ and –0.51‰) were observed in Well ZK4411/Longbizui sections respectively at the boundary between Interval II and Interval III (Fig. 6), corresponding to large-scale transgression during Cambrian Age 2. The abrupt increase of TOC, Mo concentrations, Mo/TOC ratios at the time may suggest inflow of oxic surface waters into restricted basin and the enhanced connectivity with the open ocean during large-scale transgression. In the modern Baltic Sea, the transient inflow of oxic waters into restricted basin could stimulate the operation of local Mn oxide shuttles (Huckriede and Meischner, 1996, Scholz et al., 2018). Such lower $\delta^{98/95}$Mo values are more likely a result of local Mn particulate shuttles during inflow of oxic surface waters from Cambrian open ocean into restricted basin (Fig. 7d), similar to that observed in the modern Baltic Sea (Scholz et al., 2018). During these inflow of oxygenated

seawater, isotopically light Mo were absorbed by local Mn oxides particulates, then released and delivered to anoxic sediments following the dissoluton of Mn oxides below the chemocline (Scholz et al., 2018). The local Mn shuttling of isotopically light Mo to sediments during the transient inflow of open ocean seawater into a restricted Nanhua basin was also used to explain the negative $\delta^{98/95}$Mo excursions during Ediacaran (Ostrander et al., 2019).

5.3.3. *Interval III : Mo isotope variations during the inflow of open seawater*

As mentioned earlier, during the deposition of this interval, sea level remained relatively high and the Yangtze Block began to be gradually connected with the open ocean. The inflow of trace metals into relatively restricted platform and the upwelling of H_2S-rich waters were jointly responsible for the widespread Ni-Mo sulfide ore layers across the Yangtze platform during the latest Age 2 (Lehmann et al., 2007; Wille et al., 2008; Xu et al., 2013). The $\delta^{98/95}$Mo values (0.97–0.99‰) of the Ni-Mo sulfide ore layers are comparable to the average $\delta^{98/95}$Mo values (1.13‰, n = 11) of other sulfide ores at the Maluhe, Dazhuliushui, and Sancha sections (Xu et al., 2013), which are considered to represent the $\delta^{98/95}$Mo value of contemporary seawater (Lehmann et al., 2007).

It is worthy to note that Chen et al. (2015b) reported a $\delta^{98/95}$Mo value of +2.35‰ for one Lower Cambrian black shale sample whose vertical location is<2 m above the Ni-Mo sulfide ores, indicating that the contemporary Mo isotopic composition of seawater may have approached to that of modern seawater in a short time. Based on the current thickness (80 m) of black shale and maximum timescale (7 Ma, 714–721 Ma) of Interval III, the maximum depositional rate of the black shales is estimated to be 88 kyr/m. In other words, the time interval is only about 176 kyr when the seawater $\delta^{98/95}$Mo value recorded by the Ni-Mo sulfide ores (avg. +1.13‰, Xu et al., 2013) shifted to the values recorded by the black shales (>2.0‰, Chen et al., 2015b), which is shorter than the long residence time of Mo (440 kyr) (Collier, 1985; Miller et al., 2011). Therefore the measured $\delta^{98/95}$Mo values for Ni-Mo layers at the time may not reflect the $\delta^{98/95}$Mo value of the contemporary global paleo-ocean as reported by Chen et al. (2015b). When the basin is not well connected to the open ocean and characterized with occasional seawater replenishment and intermittent dominance by continental input, the seawater $\delta^{98/95}$Mo during the deposition of Ni-Mo sulfide ores may be the expression of the mixing between the heavy $\delta^{98/95}$Mo from the open ocean and the light $\delta^{98/95}$Mo from continental input (+0.7‰). Therefore it is presumed that the Yangtze platform was freely connected with the open ocean during the deposition of black shales above Ni-Mo sulfide ores and the highest $\delta^{98/95}$Mo values recorded in the euxinic black shales (+2.35‰, Chen et al., 2015b) reflect the contemporaneous open ocean $\delta^{98/95}$Mo signal (Fig. 7e).

The $\delta^{98/95}$Mo values of Interval III generally increase from shallow shelf to deepwater region, i.e., ~ 0.0‰ on the shelf at Zunyi section, ~ +0.5‰ to +1.0‰ on the upper slope at Well ZK4411 and approaching +2.0‰ on the lower slope at Longbizui section. These results are similar to the observations of modern Black Sea where the shallower samples (<272 m water depth) under oxic/suboxic waters yield significantly lighter $\delta^{98/95}$Mo values varying from −0.6‰ to +0.9‰, whereas the deep euxinic sediments (>410 m water depth) have heavier Mo isotopic compositions (+2‰ to +2.4‰) (Neubert et al., 2008). The lower sedimentary $\delta^{98/95}$Mo values in shallow waters may reflect incomplete removal of Mo and/or a benthic oxide shuttle under oxic/suboxic waters with large Mo isotopic fractionation, while the higher sedimentary $\delta^{98/95}$Mo values in deep waters are likely related to complete Mo scavenging under euxinic conditions with small Mo isotopic fractionation (Neubert et al., 2008). Therefore, the increasing $\delta^{98/95}$Mo values from shallow water shelf to deepwater slope in this study may reflect a redox stratified ocean with oxic shallow waters and anoxic/ euxinic deep waters during early Cambrian (Fig. 7f), which is also consistent with the results determined from iron speciation data (Feng et al., 2014; Jin et al., 2016). Based on early published Mo isotope data (n = 155) from Lower Cambrian black shales, Cheng et al. (2016) reported 72% of the Mo isotopes ranging from +0.5‰ to +2‰ and proposed that the early Cambrian ocean was dominantly characterized by anoxic/euxinic deep waters with $[H_2S]_{aq} < 11$ μM.

5.4. *Implications for oceanic redox structure and oxygenation*

Enrichment pattern of redox-sensitive elements and Fe speciation data indicate preferentially euxinic waters. However, assessing absolute aqueous H_2S in the water column remains difficult.. When the variation of $\delta^{98/95}$Mo values is mainly controlled by local redox conditions, they could reflect the local seawater H_2S concentrations. While high $[H_2S]_{aq}$ content (>11 μM) promotes quantitative conversion of MoO_4^{2-} to MoS_4^{2-} with minor Mo isotopic fractionation (<0.7‰) (Siebert et al., 2003; Arnold et al., 2004; Brucker et al., 2009), low $[H_2S]_{aq}$ (<11 μM) leads to incomplete conversion of molybdate with large Mo isotopic fractionation (up to 3‰) (Helz et al., 1996). Note that the variations in $\delta^{98/95}$Mo values of seawater are closely related to changes in the oceanic Mo reservoir size (Wille et al., 2008; Dahl et al., 2010). The high and relatively stable Mo concentrations from samples at Well ZK4411 and other sections in Interval I and III may imply no significant changes in seawater Mo reservoir size, and further suggest no or minor changes in contemporaneous seawater Mo isotopes in the timesframe of Interval I and Interval III. In addition, the high Mo/TOC ratios in Interval I and III indicate that the Yangtze Block was well connected with open ocean rather than restricted/semi-restricted basin, and thus there may be little or minor changes of seawater Mo isotopes. Therefore, it is appropriate to infer the minimum $\delta^{98/95}$Mo value of contemporaneous seawater from the heaviest sedimentary $\delta^{98/95}$Mo values (i.e., $\delta^{98/95}Mo_{Sediment} \leq \delta^{98/95}Mo_{Seawater}$) across the studied timeframe, and the variable sedimentary $\delta^{98/95}$Mo values most likely reflect Mo isotopic fractionation relative to the contemporaneous seawater. Based on $\delta^{98/95}$Mo data from this study and the published data at Zunyi and Three Gorges sections in shallow shelf (Xu et al., 2012; Kendall et al., 2015; Wen et al., 2015), Longbizui, Rongxi, and Wuhe sections in the slope regions (Chen et al., 2015b; Och et al., 2016; Ostrander et al., 2019) (Fig. 6), the heaviest $\delta^{98/95}$Mo value (ca. +2.08‰) observed at Three Gorges section in the Interval I has the smallest isotope fractionation and thus reflects euxinic waters with $[H_2S]_{aq} > 11$ μM in the shallow shelf (Fig. 7b). By contrast, the variable $\delta^{98/95}$Mo values (from +0.2‰ to +1.32‰) with large isotope fractionation at Well ZK4411 and Rongxi /Wuhe sections may indicate euxinic waters with low H_2S concentration (Fig. 7b). Similarly, higher $\delta^{98/95}$Mo values (ca. +1.94‰) in Interval III at Longbizui section in the lower slope region may reflect a small Mo isotope fractionation with relatively high H_2S concentration in the deep anoxic waters (Fig. 7f). Such a redox structure with euxinic waters ($[H_2S]_{aq} > 11$ μM) sandwiched by oxic surface waters and anoxic deep waters is also consistent with oceanic redox models during E-C transition as proposed by Feng et al. (2014) and Cheng et al. (2016).

The modern well-oxygenated ocean is uniformly enriched in heavy Mo isotopes ($\delta^{98/95}$Mo = 2.34 ± 0.10‰, Siebert et al., 2003) relative to riverine inputs ($\delta^{98/95}$Mo = +0.7‰) (Archer and Vance, 2008). The preferential adsorption of isotopically light Mo by Fe–Mn oxides in oxygenated waters may result in large isotopic fractionation of up to 3‰ (Barling et al., 2001; Goldberg et al., 2009). Thus, heavier seawater Mo isotopic compositions are commonly used to reflect oxygenated paleo-oceans, while low seawater $\delta^{98/95}$Mo values indicate extensive anoxia (Arnold et al., 2004; Wille et al., 2007; Dahl et al., 2010; Wen et al., 2011; Chen et al., 2015b; Kendall et al., 2015; Yin et al., 2018). Based on the near-modern seawater $\delta^{98/95}$Mo values (≥2.0‰) for a few Ediacaran-Cambrian euxinic black shales in Yangtze Block, Chen et al. (2015b) and Kendall et al. (2015) suggested that there were at least transient episodes of extensive ocean oxygenation at the time. The iron speciation and trace elements data, however, suggest anoxic and/or euxinic deep waters in some regions of Yangtze Block during this period (Wang et al., 2012; Feng et al., 2014; Sperling et al., 2015). Actually, the shuttling of isotopically light Mo to euxinic sediments by Mn oxides in

the redox stratified Ediacaran-Cambrian ocean may lead to heavier seawater Mo isotopes. Although the quantitative estimation of this effect on driving heavy seawater Mo isotopes is difficult, it may at least contribute to heterogeneous heavy seawater Mo isotopes in local areas before being mixed with global paleo-ocean. In addition, removal of lighter-mass Mo isotopes from widespread H_2S-poor Ediacaran-Cambrian ocean may also drive a heavy seawater $\delta^{98/95}$Mo value (Cheng et al, 2016). These two mechanisms may jointly play a significant role in driving heterogeneous heavy seawater $\delta^{98/95}$Mo values for the redox stratified Ediacaran-Cambrian ocean in the Yangtze Block of South China. This may also partly explain why the near-modern $\delta^{98/95}$Mo values (>2‰) are recorded by only 4% (2 of 52) of the euxinic early Cambrian samples examined by Cheng et al. (2016) and by only a few euxinic samples during late Ediacaran (Kendall et al., 2015). In this sense, local depositional environments and their effects on heterogeneous seawater Mo isotopes should be considered before heavy sedimentary $\delta^{98/95}$Mo records are applied to trace the oxygenation state of global E-C paleo-ocean.

6. Conclusions

The $\delta^{98/95}$Mo and $\delta^{13}C_{org}$ values, TOC, as well as trace and elements concentrations of continuous fresh core shale samples were analyzed to reconstruct the paleo-ocean redox structure across the Yangtze Block during the E-C transition. The main conclusions are summarized below.

(1) The redox stratified ocean with oxic surface waters and anoxic/euxinic deep waters prevailed across the E-C transition (Interval I). The oxic surface waters may spread to the upper slope region during Cambrian Fortunian and Age 2 (Interval II). Afterwards, anoxic with intermittently euxinic deep waters occurred during latest Age 2 and early Age 3 (Interval III).
(2) The Yangtze platform was well connected with the open ocean during late Ediacaran, and then became strongly restricted during Cambrian Fortunian and Age 2. Afterwards, a large-scale transgression during latest Age 2 enhanced the connectivity with the open ocean, and oxic waters plus nutrients and trace metals flowed into restricted basin.
(3) The negative $\delta^{98/95}$Mo values may reflect preferential adsorption of isotopically light Mo by Mn oxides particles above the chemocline and their subsequent shuttling to euxinic sediments in the redox stratified late Ediacaran ocean; whereas the relatively low $\delta^{98/95}$Mo values during Cambrian Fortunian and Age 2 indicate the decrease of $\delta^{98/95}Mo_{Seawater}$ values in the restricted basin. In conjunction with published Mo isotope data, the variations of sedimentary $\delta^{98/95}$Mo values from shallow shelf to deepwater slope regions draw the outline of 'sandwich'-like model with euxinic waters ($[H_2S]_{aq} > 11$ μM) sandwiched by oxic surface waters and anoxic deep waters during the E-C transition.
(4) The adsorption of isotopically light Mo by Mn oxides may lead to heavier seawater Mo isotopes and also likely has played a role in driving locally heterogeneous heavy seawater $\delta^{98/95}$Mo values of redox stratified Ediacaran-Cambrian ocean in the Yangtze Block of South China.

Declaration of Competing Interest

The authors declare that they have no known competing financial interests or personal relationships that could have appeared to influence the work reported in this paper.

Acknowledgments

This study was jointly supported by Natural Science Foundation of China (Grant No. 41925014) and the National Science and Technology Major Project (2017zx05008-002-004). Three anonymous reviewers and the Precambrian Research editor Prof. Frances Westall are thanked for their constructive comments and suggestions that have greatly improved the whole quality and clarity of the manuscript. This is contribution No.IS-3005 from GIGCAS.

References

Algeo, T.J., Li, C., 2020. Redox classification and calibration of redox thresholds in sedimentary systems. Geochim. Cosmochim. Acta 287, 8–26.
Algeo, T.J., Lyons, T.W., 2006. Mo-total organic carbon covariation in modern anoxic marine environments: Implications for analysis of paleoredox and paleohydrographic conditions. Paleoceanography 21, PA1016.
Algeo, T.J., Maynard, J.B., 2004. Trace-element behavior and redox facies in core shales of Upper Pennsylvanian Kansas-type cyclothems. Chem. Geol. 206, 289–318.
Algeo, T.J., Rowe, H., 2012. Paleoceanographic applications of trace-metal concentration data. Chem. Geol. 324–325, 6–18.
Algeo, T.J., Tribovillard, N., 2009. Environmental analysis of paleoceanographic systems based on molybdenum-uranium covariation. Chem. Geol. 268, 211–225.
Al-Husseini, M., Ruebsam, W., 2020. Interpreting Phanerozoic δ13C patterns as periodic glacio-eustatic sequences. In: Montenari, M. (Ed.), Stratigraphy & Timescales, Volume 5, Case Studies in Isotope Stratigraphy, p. 41–106.
Amthor, J.E., Grotzinger, J.P., Schroder, S., Bowring, S.A., Ramezani, J., Martin, M.W., Matter, A., 2003. Extinction of Cloudina and Namacalathus at the Precambrian-Cambrian boundary in Oman. Geology 31, 431–434.
An, Z.H., Jiang, G.Q., Tong, J.N., Tian, L., Ye, Q., Song, H.Y., Song, H.J., 2015. Stratigraphic position of the Ediacaran Miaohe biota and its constrains on the age of the upper Doushantuo $\delta^{13}C$ anomaly in the Yangtze Gorges area, South China. Precambr. Res. 271, 243–253.
Anbar, A.D., 2004. Molybdenum stable isotopes: Observations, interpretations and directions, in: Johnson, C.M., Beard, B.L., Albarede, F. (Eds.), Geochemistry of Non-Traditional Stable Isotopes, pp. 429–454.
Archer, C., Vance, D., 2008. The isotopic signature of the global riverine molybdenum flux and anoxia in the ancient oceans. Nat. Geosci. 1, 597–600.
Arnold, G.L., Anbar, A.D., Barling, J., Lyons, T.W., 2004. Molybdenum isotope evidence for widespread anoxia in mid-proterozoic oceans. Science 304, 87–90.
Babcock, L.E., Peng, S.-C., Brett, C.E., Zhu, M.-Y., Ahlberg, P., Bevis, M., Robison, R.A., 2015. Global climate, sea level cycles, and biotic events in the Cambrian Period. Palaeoworld 24, 5–15.
Barling, J., Arnold, G.L., Anbar, A.D., 2001. Natural mass-dependent variations in the isotopic composition of molybdenum. Earth Planet. Sci. Lett. 193, 447–457.
Canfield, D.E., Poulton, S.W., Knoll, A.H., Narbonne, G.M., Ross, G., Goldberg, T., Strauss, H., 2008. Ferruginous conditions dominated later Neoproterozoic deep-water chemistry. Science 321, 949–952.
Canfield, D.E., Poulton, S.W., Narbonne, G.M., 2007. Late-Neoproterozoic deep-ocean oxygenation and the rise of animal life. Science 315, 92–95.
Calvert, S.E., Pedersen, T.F., 1996. Sedimentary geochemistry of manganese: Implications for the environment of formation of manganiferous black shales. Econnmic Geology 91, 36–47.
Chang, H., Chu, X., Feng, L., Huang, J., Chen, Y., 2018. Marine redox stratification on the earliest Cambrian (ca. 542–529 Ma) Yangtze Platform. Palaeogeogr. Palaeoclimatol. Palaeoecol. 504, 75–85.
Charvet, J., 2013. The Neoproterozoic-Early Paleozoic tectonic evolution of the South China Block: An overview. J. Asian Earth Sci. 74, 198–209.
Chen, D., Wang, J., Qing, H., Yan, D., Li, R., 2009. Hydrothermal venting activities in the Early Cambrian, South China: Petrological, geochronological and stable isotopic constraints. Chem. Geol. 258, 168–181.
Chen, D., Zhou, X., Fu, Y., Wang, J., Yan, D., 2015a. New U-Pb zircon ages of the Ediacaran-Cambrian boundary strata in South China. Terra Nova 27, 62–68.
Chen, X., Ling, H.F., Vance, D., Shields-Zhou, G.A., Zhu, M., Poulton, S.W., Och, L.M., Jiang, S.Y., Li, D., Cremonese, L., Archer, C., 2015b. Rise to modern levels of ocean oxygenation coincided with the Cambrian radiation of animals. Nature Communication 6, 7142.
Cheng, M., Li, C., Chen, X., Zhou, L., Algeo, T.J., Ling, H.-F., Feng, L.-J., Jin, C.-S., 2018. Delayed Neoproterozoic oceanic oxygenation: Evidence from Mo isotopes of the Cryogenian Datangpo Formation. Precambr. Res. 319, 187–197.
Cheng, M., Li, C., Zhou, L., Algeo, T.J., Zhang, F., Romaniello, S., Jin, C.-S., Lei, L.-D., Feng, L.-J., Jiang, S.-Y., 2016. Marine Mo biogeochemistry in the context of dynamically euxinic mid-depth waters: A case study of the lower Cambrian Niutitang shales, South China. Geochim. Cosmochim. Acta 183, 79–93.
Collier, R.W., 1985. Molybdenum in the Northeast Pacific Ocean. Limnol. Oceanogr. 30, 1351–1354.
Compston, W., Zhang, Z., Cooper, J.A., Ma, G., Jenkins, R.J.F., 2008. Further SHRIMP geochronology on the early Cambrian of south China. Am. J. Sci. 308, 399–420.
Condon, D., Zhu, M.Y., Bowring, S., Wang, W., Yang, A.H., Jin, Y.G., 2005. U-Pb ages from the neoproterozoic Doushantuo Formation, China. Science 308, 95–98.
Cremonese, L., Shields-Zhou, G., Struck, U., Ling, H.-F., Och, L., Chen, X., Li, D., 2013. Marine biogeochemical cycling during the early Cambrian constrained by a nitrogen and organic carbon isotope study of the Xiaotan section, South China. Precambrian Research 225, 148–165.
Crusius, J., Calvert, S., Pedersen, T., Sage, D., 1996. Rhenium and molybdenum enrichments in sediments as indicators of oxic, suboxic, and sulfidic conditions of deposition. Earth Planet. Sci. Lett. 145, 65–78.

Crusius, J., Thomson, J., 2000. Comparative behavior of authigenic Re, U, and Mo during reoxidation and subsequent long-term burial in marine sediments. Geochim. Cosmochim. Acta 64, 2233–2242.
Dahl, T.W., Anbar, A.D., Gordon, G.W., Rosing, M.T., Frei, R., Canfield, D.E., 2010. The behavior of molybdenum and its isotopes across the chemocline and in the sediments of sulfidic Lake Cadagno, Switzerland. Geochim. Cosmochim. Acta 74, 144–163.
Dahl, T.W., Canfield, D.E., Rosing, M.T., Frei, R.E., Gordon, G.W., Knoll, A.H., Anbar, A. D., 2011. Molybdenum evidence for expansive sulfidic water masses in similar to 750 Ma oceans. Earth Planet. Sci. Lett. 311, 264–274.
Dellwig, O., Leipe, T., März, C., Glockzin, M., Pollehne, F., Schnetger, B., Yakushev, E.V., Böttcher, M.E., Brumsack, H.J., 2010. A new particulate Mn–Fe–P-shuttle at the redoxcline of anoxic basins. Geochim. Cosmochim. Acta 74, 7100–7115.
Fan, H., Wen, H., Zhu, X., 2016. Marine Redox Conditions in the Early Cambrian Ocean: Insights from the Lower Cambrian Phosphorite Deposits, South China. J. Earth Sci. 27, 282–296.
Fang, X., Wu, L., Geng, A., Deng, Q., 2019. Formation and evolution of the Ediacaran to Lower Cambrian black shales in the Yangtze Platform, South China. Palaeogeogr. Palaeoclimatol. Palaeoecol. 527, 87–102.
Feng, L., Li, C., Huang, J., Chang, H., Chu, X., 2014. A sulfate control on marine mid-depth euxinia on the early Cambrian (ca. 529–521Ma) Yangtze platform. South China. Precambrian Research 246, 123–133.
Fike, D.A., Grotzinger, J.P., Pratt, L.M., Summons, R.E., 2006. Oxidation of the Ediacaran Ocean. Nature 444, 744–747.
Fu, Y., Dong, L., Li, C., Qu, W., Pei, H., Qiao, W., Shen, B., 2016. New Re-Os isotopic constrains on the formation of the metalliferous deposits of the Lower Cambrian Niutitang formation. J. Earth Sci. 27, 271–281.
Gao, P., He, Z., Li, S., Lash, G.G., Li, B., Huang, B., Yan, D., 2018. Volcanic and hydrothermal activities recorded in phosphate nodules from the Lower Cambrian Niutitang Formation black shales in South China. Palaeogeogr. Palaeoclimatol. Palaeoecol. 505, 381–397.
Gao, P., Liu, G., Jia, C., Young, A., Wang, Z., Wang, T., Zhang, P., Wang, D., 2016. Redox variations and organic matter accumulation on the Yangtze carbonate platform during Late Ediacaran-Early Cambrian: Constraints from petrology and geochemistry. Palaeogeogr. Palaeoclimatol. Palaeoecol. 450, 91–110.
Goldberg, T., Archer, C., Vance, D., Poulton, S.W., 2009. Mo isotope fractionation during adsorption to Fe (oxyhydr) oxides. Geochim. Cosmochim. Acta 73, 6502–6516.
Goldberg, T., Strauss, H., Guo, Q., Liu, C., 2007. Reconstructing marine redox conditions for the early Cambrian Yangtze Platform: Evidence from biogenic sulphur and organic carbon isotopes. Palaeogeogr. Palaeoclimatol. Palaeoecol. 254, 175–193.
Guo, Q., Strauss, H., Liu, C., Goldberg, T., Zhu, M., Pi, D., Heubeck, C., Vernhet, E., Yang, X., Fu, P., 2007. Carbon isotopic evolution of the terminal Neoproterozoic and early Cambrian: evidence from the Yangtze Platform, South China. Palaeogeogr. Palaeoclimatol. Palaeoecol. 254, 140–157.
Guo, Q., Strauss, H., Zhu, M., Zhang, J., Yang, X., Lu, M., Zhao, F., 2013. High resolution organic carbon isotope stratigraphy from a slope to basinal setting on the Yangtze Platform, South China: implications for the Ediacaran-Cambrian transition. Precambr. Res. 225, 209–217.
Hatch, J.R., Leventhal, J.S., 1992. Relationship between inferred redox potential of the depositional environment and geochemistry of the Upper Pennsylvanian (Missourian) Stark Shale Member of the Dennis Limestone, Wabaunsee County, Kansas, USA. Chem. Geol. 99, 65–82.
Helz, G.R., Miller, C.V., Charnock, J.M., Mosselmans, J.F.W., Pattrick, R.A.D., Garner, C. D., Vaughan, D.J., 1996. Mechanism of molybdenum removal from the sea and its concentration in black shales: EXAFS evidence. Geochim. Cosmochim. Acta 60, 3631–3642.
Huckriede, H., Meischner, D., 1996. Origin and environment of manganese-rich sediments within black-shale basin. Geochim. Cosmochim. Acta 60, 1399–1413.
Jiang, G., Shi, X., Zhang, S., Wang, Y., Xiao, S., 2011. Stratigraphy and paleogeography of the Ediacaran Doushantuo Formation (ca. 635–551 Ma) in South China. Gondwana Res. 19, 831–849.
Jiang, S.-Y., Chen, Y.-Q., Ling, H.-F., Yang, J.-H., Feng, H.-Z., Ni, P., 2006. Trace- and rare-earth element geochemistry and Pb–Pb dating of black shales and intercalated Ni–Mo–PGE–Au sulfide ores in Lower Cambrian strata, Yangtze Platform, South China. Miner. Deposita 41, 453–467.
Jiang, S.-Y., Pi, D.-H., Heubeck, C., Frimmel, H., Liu, Y.-P., Deng, H.-L., Ling, H.-F., Yang, J.-H., 2009. Early Cambrian ocean anoxia in South China. Nature 459, E5–E6.
Jiang, S.-Y., Yang, J.-H., Ling, H.-F., Chen, Y.-Q., Feng, H.-Z., Zhao, K.-D., Ni, P., 2007. Extreme enrichment of polymetallic Ni–Mo–PGE–Au in Lower Cambrian black shales of South China: An Os isotope and PGE geochemical investigation. Palaeogeogr. Palaeoclimatol. Palaeoecol. 254, 217–228.
Jin, C., Li, C., Algeo, T.J., Planavsky, N.J., Cui, H., Yang, X., Zhao, Y., Zhang, X., Xie, S., 2016. A highly redox-heterogeneous ocean in South China during the early Cambrian (~ 529–514 Ma): Implications for biota-environment co-evolution. Earth Planet. Sci. Lett. 441, 38–51.
Jones, B., Manning, D.A.C., 1994. Comparison of geochemical indexes used for the interpretation of paleoredox conditions in ancient mudstones. Chem. Geol. 111, 111–129.
Kendall, B., Komiya, T., Lyons, T.W., Bates, S.M., Gordon, G.W., Romaniello, S.J., Jiang, G., Creaser, R.A., Xiao, S., McFadden, K., Sawaki, Y., Tahata, M., Shu, D., Han, J., Li, Y., Chu, X., Anbar, A.D., 2015. Uranium and molybdenum isotope evidence for an episode of widespread ocean oxygenation during the late Ediacaran Period. Geochim. Cosmochim. Acta 156, 173–193.
Kendall, B., Dahl, T.W., Anbar, A.D., 2017. Good Golly, Why Moly? The stable isotope geochemistry of molybdenum. Rev. Mineral. Geochem. 82, 683–732.
Kimura, H., Watanabe, Y., 2001. Oceanic anoxia at the Precambrian-Cambrian boundary. Geology 29, 995–998.
King, E.K., Pett-Ridge, J.C., 2018. Reassessing the dissolved molybdenum isotopic composition of ocean inputs: The effect of chemical weathering and groundwater. Geology 46, 955–958.
Knoll, A.H., Carroll, S.B., 1999. Early animal evolution: Emerging views from comparative biology and geology. Science 284, 2129–2137.
Lehmann, B., Naegler, T.F., Holland, H.D., Wille, M., Mao, J., Pan, J., Ma, D., Dulski, P., 2007. Highly metalliferous carbonaceous shale and Early Cambrian seawater. Geology 35, 403–406.
Li, C., Love, G.D., Lyons, T.W., Fike, D.A., Sessions, A.L., Chu, X., 2010. A stratified redox model for the Ediacaran ocean. Science 328, 80–83.
Li, C., Love, G.D., Lyons, T.W., Scott, C.T., Feng, L., Huang, J., Chang, H., Zhang, Q., Chu, X., 2012. Evidence for a redox stratified Cryogenian marine basin, Datangpo Formation, South China. Earth Planet. Sci. Lett. 331–332, 246–256.
Li, J., Liang, X.-R., Zhong, L.-F., Wang, X.-C., Ren, Z.-Y., Sun, S.-L., Zhang, Z.-F., Xu, J.-F., 2014. Measurement of the isotopic composition of molybdenum in geological samples by MC-ICP-MS using a novel chromatographic extraction technique. Geostand. Geoanal. Res. 38, 345–354.
Li, X.-H., Li, W.-X., Li, Z.-X., Lo, C.-H., Wang, J., Ye, M.-F., Yang, Y.-H., 2009. Amalgamation between the Yangtze and Cathaysia Blocks in South China: Constraints from SHRIMP U-Pb zircon ages, geochemistry and Nd-Hf isotopes of the Shuangxiwu volcanic rocks. Precambr. Res. 174, 117–128.
Li, Z.X., Bogdanova, S.V., Collins, A.S., Davidson, A., De Waele, B., Ernst, R.E., Fitzsimons, I.C.W., Fuck, R.A., Gladkochub, D.P., Jacobs, J., Karlstrom, K.E., Lu, S., Natapov, L.M., Pease, V., Pisarevsky, S.A., Thrane, K., Vernikovsky, V., 2008. Assembly, configuration, and break-up history of Rodinia: A synthesis. Precambr. Res. 160, 179–210.
Linnemann, U., Ovtcharova, M., Schaltegger, U., Gartner, A., Hautmann, M., Geyer, G., Vickers-Rich, P., Rich, T., Plessen, B., Hofmann, M., 2019. New high-resolution age data from the Ediacaran-Cambrian boundary indicate rapid, ecologically driven onset of the Cambrian explosion. Terra Nova 31, 49–58.
Liu, J.S., Algeo, T.J., 2020. Beyond redox: Control of trace-metal enrichment in anoxic marine facies by watermass chemistry and sedimentation rate. Geochim. Cosmochim. Acta 7, 296–317.
Marshall, C.R., 2006. Explaining the Cambrian "Explosion" of Animals. Annu. Rev. Earth Planet. Sci. 34, 355–384.
Miller, C.A., Peucker-Ehrenbrink, B., Walker, B.D., Marcantonio, F., 2011. Re-assessing the surface cycling of molybdenum and rhenium. Geochim. Cosmochim. Acta 75, 7146–7179.
Morford, J.L., Martin, W.R., Francois, R., Carney, C.M., 2009. A model for uranium, rhenium, and molybdenum diagenesis in marine sediments based on results from coastal locations. Geochim. Cosmochim. Acta 73, 2938–2960.
Nägler, T.F., Anbar, A.D., Archer, C., Goldberg, T., Gordon, G.W., Greber, N.D., Siebert, C., Sohrin, Y., Vance, D., 2014. Proposal for an international molybdenum isotope measurement standard and data representation. Geostands and Geoanalytical Research 38, 149–151.
Neubert, N., Nägler, T.F., Böttcher, M.E., 2008. Sulfidity controls molybdenum isotope fractionation into euxinic sediments: evidence from the modern Black Sea. Geology 36, 775–778.
Och, L.M., Cremonese, L., Shields-Zhou, G.A., Poulton, S.W., Struck, U., Ling, H., Li, D., Chen, X., Manning, C., Thirlwall, M., Strauss, H., Zhu, M., 2016. Palaeoceanographic controls on spatial redox distribution over the Yangtze Platform during the Ediacaran-Cambrian transition. Sedimentology 63, 378–410.
Och, L.M., Shields-Zhou, G.A., 2012. The Neoproterozoic oxygenation event: Environmental perturbations and biogeochemical cycling. Earth Sci. Rev. 110, 26–57.
Och, L.M., Shields-Zhou, G.A., Poulton, S.W., Manning, C., Thirlwall, M.F., Li, D., Chen, X., Ling, H., Osborn, T., Cremonese, L., 2013. Redox changes in Early Cambrian black shales at Xiaotan section, Yunnan Province, South China. Precambr. Res. 225, 166–189.
Ostrander, C.M., Sahoo, S.K., Kendall, B., Jiang, G., Planavsky, N.J., Lyons, T.W., Nielsen, S.G., Owens, J.D., Gordon, G.W., Romaniello, S.J., Anbar, A.D., 2019. Multiple negative molybdenum isotope excursions in the Doushantuo Formation (South China) fingerprint complex redox-related processes in the Ediacaran Nanhua Basin. Geochim. Cosmochim. Acta 261, 191–209.
Ostrander, C.M., Kendall, B., Olson, S.L., Lyons, T.W., Gordon, G.W., Romaniello, S.J., Zheng, W., Reinhard, C.T., Roy, M., Anbar, A.D., 2020. An expanded shale δ^{98}Mo record permits recurrent shallow marine oxygenation during the Neoarchean. Chem. Geol. 532, 119391.
Pearce, C.R., Cohen, A.S., Coe, A.L., Burton, K.W., 2008. Molybdenum isotope evidence for global ocean anoxia coupled with perturbations to the carbon cycle during the Early Jurassic. Geology 36, 231–234.
Pi, D.-H., Liu, C.-Q., Shields-Zhou, G.A., Jiang, S.-Y., 2013. Trace and rare earth element geochemistry of black shale and kerogen in the early Cambrian Niutitang Formation in Guizhou province, South China: Constraints for redox environments and origin of metal enrichments. Precambr. Res. 225, 218–229.
Poulton, S.W., Fralick, P.W., Canfield, D.E., 2010. Spatial variability in oceanic redox structure 1.8 billion years ago. Nat. Geosci. 3, 486–490.
Poulson Brucker, R.L., McManus, J., Severmann, S., Berelson, W.M., 2009. Molybdenum behavior during early diagenesis: Insights from Mo isotopes. Geochem. Geophys. Geosyst. 10, Q06010.
Reinhard, C.T., Raiswell, R., Scott, C., Anbar, A.D., Lyons, T.W., 2009. A Late Archean Sulfidic Sea Stimulated by Early Oxidative Weathering of the Continents. Science 326, 713–716.
Ruebsam, W., Dickson, A.J., Hoyer, E.M., Schwark, L., 2017. Multiproxy reconstruction of oceanographic conditions in the southern epeiric Kupferschiefer Sea (Late

Permian) based on redox-sensitive trace elements, molybdenum isotopes and biomarkers. Gondwana Res. 44, 205–218.
Sahoo, S.K., 2015. Ediacaran ocean redox evolution. UNLV Theses, Dissertations 2577.
Sahoo, S.K., Planavsky, N.J., Jiang, G., Kendall, B., Owens, J.D., Wang, X., Shi, X., Anbar, A.D., Lyons, T.W., 2016. Oceanic oxygenation events in the anoxic Ediacaran ocean. Geobiology 14, 457–468.
Scholz, F., Baum, M., Siebert, C., Eroglu, S., Dale, A.W., Naumann, M., Sommer, S., 2018. Sedimentary molybdenum cycling in the aftermath of seawater inflow to the intermittently euxinic Gotland Deep, Central Baltic Sea. Chem. Geol. 491, 27–38.
Scholz, F., McManus, J., Sommer, S., 2013. The manganese and iron shuttle in a modern euxinic basin and implications for molybdenum cycling at euxinic ocean margins. Chem. Geol. 355, 56–68.
Scholz, F., Hensen, C., Noffke, A., Rohde, A., Liebetrau, V., Wallmann, K., 2011. Early diagenesis of redox-sensitive trace metals in the Peru upwelling area – response to ENSO-related oxygen fluctuations in the water column. Geochim. Cosmochim. Acta 75, 7257–7276.
Scott, C., Lyons, T.W., Bekker, A., Shen, Y., Poulton, S.W., Chu, X., Anbar, A.D., 2008. Tracing the stepwise oxygenation of the Proterozoic ocean. Nature 452, 456–459.
Shen, Y.N., Zhao, R., Chu, X.L., Lei, J.J., 1998. The carbon and sulfur isotope signatures in the Precambrian-Cambrian transition series of the Yangtze Platform. Precambr. Res. 89, 77–86.
Shu, L., 2012. An analysis of principal features of tectonic evolution in South China Block. Geological Bulletin of China 31, 1035–1053 (in Chinese with English abstract).
Siebert, C., Nägler, T.F., von Blanckenburg, F., Kramers, J.D., 2003. Molybdenum isotope records as a potential new proxy for paleoceanography. Earth Planet. Sci. Lett. 211, 159–171.
Siebert, C., Pett-Ridge, J.C., Opfergelt, S., Guicharnaud, R.A., Halliday, A.N., Burton, K. W., 2015. Molybdenum isotope fractionation in soils: Influence of redox conditions, organic matter, and atmospheric inputs. Geochim. Cosmochim. Acta 162, 1–24.
Sperling, E.A., Wolock, C.J., Morgan, A.S., Gill, B.C., Kunzmann, M., Halverson, G.P., Macdonald, F.A., Knoll, A.H., Johnston, D.T., 2015. Statistical analysis of iron geochemical data suggests limited late Proterozoic oxygenation. Nature 523, 451–454.
Steiner, M., Li, G., Qian, Y., Zhu, M., Erdtmann, B.-D., 2007. Neoproterozoic to early Cambrian small shelly fossil assemblages and a revised biostratigraphic correlation of the Yangtze Platform (China). Palaeogeogr. Palaeoclimatol. Palaeoecol. 254, 67–99.
Steiner, M., Wallis, E., Erdtmann, B.D., Zhao, Y.L., Yang, R.D., 2001. Submarine-hydrothermal exhalative ore layers in black shales from South China and associated fossils - insights into a Lower Cambrian facies and bio-evolution. Palaeogeogr. Palaeoclimatol. Palaeoecol. 169, 165–191.
Taylor, S.R., McLennan, S.M., 1985. The Continental Crust: Its Composition and Evolution. Blackwell Scientific Publications, Oxford, p. 311.
Tribovillard, N., Algeo, T.J., Baudin, F., Riboulleau, A., 2012. Analysis of marine environmental conditions based on molybdenum–uranium covariation—Applications to Mesozoic paleoceanography. Chem. Geol. 324–325, 46–58.
Tribovillard, N., Algeo, T.J., Lyons, T., Riboulleau, A., 2006. Trace metals as paleoredox and paleoproductivity proxies: An update. Chem. Geol. 232, 12–32.
Turgeon, S., Brumsack, H.J., 2006. Anoxic vs dysoxic events reflected in sediment geochemistry during the Cenomanian-Turonian Boundary Event (Cretaceous) in the Umbria–Marche Basin of central Italy. Chem. Geol. 234, 321–339.
Wang, D., Struck, U., Ling, H.-F., Guo, Q.-J., Shields-Zhou, G.A., Zhu, M.-Y., Yao, S.-P., 2015a. Marine redox variations and nitrogen cycle of the early Cambrian southern margin of the Yangtze Platform, South China: Evidence from nitrogen and organic carbon isotopes. Precambr. Res. 267, 209–226.
Wang, J., Chen, D., Yan, D., Wei, H., Xiang, L., 2012. Evolution from an anoxic to oxic deep ocean during the Ediacaran-Cambrian transition and implications for bioradiation. Chem. Geol. 306–307, 129–138.
Wang, J., Li, Z.X., 2003. History of Neoproterozoic rift basins in South China: implications for Rodinia break-up. Precambr. Res. 122, 141–158.
Wang, X., Shi, X., Zhao, X., Tang, D., 2015b. Increase of seawater Mo inventory and ocean oxygenation during the early Cambrian. Palaeogeogr. Palaeoclimatol. Palaeoecol. 440, 621–631.
Wen, H., Carignan, J., Zhang, Y., Fan, H., Cloquet, C., Liu, S., 2011. Molybdenum isotopic records across the Precambrian-Cambrian boundary. Geology 39, 775–778.
Wen, H., Fan, H., Zhang, Y., Cloquet, C., Carignan, J., 2015. Reconstruction of early Cambrian ocean chemistry from Mo isotopes. Geochim. Cosmochim. Acta 164, 1–16.
Wignall, P.B., Twitchett, R.J., 1996. Oceanic anoxia and the end Permian mass extinction. Science 272, 1155–1158.
Wille, M., Kramers, J.D., Nägler, T.F., Beukes, N.J., Schröder, S., Meisel, T., Lacassie, J.P., Voegelin, A.R., 2007. Evidence for a gradual rise of oxygen between 2.6 and 2.5 Ga from Mo isotopes and Re-PGE signatures in shales. Geochim. Cosmochim. Acta 71, 2417–2435.
Wille, M., Naegler, T.F., Lehmann, B., Schroeder, S., Kramers, J.D., 2008. Hydrogen sulphide release to surface waters at the Precambrian/Cambrian boundary. Nature 453, 767–769.
Willbold, M., Elliott, T., 2017. Molybdenum isotope variations in magmatic rocks. Chem. Geol. 449, 253–268.
Xiang, L., Schoepfer, S.D., Shen, S.-Z., Cao, C.-Q., Zhang, H., 2017. Evolution of oceanic molybdenum and uranium reservoir size around the Ediacaran-Cambrian transition: Evidence from western Zhejiang, South China. Earth Planet. Sci. Lett. 464, 84–94.
Xu, L., Lehmann, B., Mao, J., 2013. Seawater contribution to polymetallic Ni–Mo–PGE–Au mineralization in Early Cambrian black shales of South China: Evidence from Mo isotope, PGE, trace element, and REE geochemistry. Ore Geol. Rev. 52, 66–84.
Xu, L., Lehmann, B., Mao, J., Nägler, T.F., Neubert, N., Böttcher, M.E., Escher, P., 2012. Mo isotope and trace element patterns of Lower Cambrian black shales in South China: Multi-proxy constraints on the paleoenvironment. Chem. Geol. 318–319, 45–59.
Xu, L., Lehmann, B., Mao, J., Qu, W., Du, A., 2011. Re-Os age of polymetallic Ni-Mo-PGE-Au mineralization in early Cambrian black shales of South China-a reassessment. Econ. Geol. 106, 511–522.
Yang, B., Steiner, M., Li, G., Keupp, H., 2014. Terreneuvian small shelly faunas of East Yunnan (South China) and their biostratigraphic implications. Palaeogeogr. Palaeoclimatol. Palaeoecol. 398.
Yeasmin, R., Chen, D., Fu, Y., Wang, J., Guo, Z., Guo, C., 2017. Climatic-oceanic forcing on the organic accumulation across the shelf during the Early Cambrian (Age 2 through 3) in the mid-upper Yangtze Block, NE Guizhou, South China. J. Asian Earth Sci. 134, 365–386.
Yin, L., Li, J., Tian, H., Long, X., 2018. Rhenium-osmium and molybdenum isotope systematics of black shales from the Lower Cambrian Niutitang Formation, SW China: Evidence of a well oxygenated ocean at ca. 520 Ma. Chem. Geol. 499, 26–42.
Zhai, L., Wu, C., Ye, Y., Zhang, S., An, Z., 2018. Marine redox variations during the Ediacaran-Cambrian transition on the Yangtze Platform, South China. Geol. J. 53, 58–79.
Zhang, S.H., Jiang, G.Q., Zhang, J.M., Song, B., Kennedy, M.J., Christie-Blick, N., 2005. U-Pb sensitive high-resolution ion microprobe ages from the Doushantuo Formation in south China: Constraints on late Neoproterozoic glaciations. Geology 33, 473–476.
Zhang, J.P., Fan, T.L., Zhang, Y.D., Lash, G.G., Li, Y.F., Wu, Y., 2017. Heterogenous oceanic redox conditions through the Ediacaran-Cambrian boundary limited the metazoan zonation. Sci. Rep. 7, 8550.
Zhang, F.F., Xiao, S.H., Romaniello, S.J., Hardisty, D., Li, C., Melezhik, V., Pokrovsky, B., Cheng, M., Shi, W., Lenton, T.M., 2019. Global marine redox changes drove the rise and fall of the Ediacara biota. Geobiology 17, 594–610.
Zhao, P.-P., Li, J., Zhang, L., Wang, Z.-B., Kong, D.-X., Ma, J.-L., Wei, G.-J., Xu, J.-F., 2016. Molybdenum Mass Fractions and Isotopic Compositions of International Geological Reference Materials. Geostand. Geoanal. Res. 40, 217–226.
Zhu, M.-Y., Babcock, L.E., Peng, S.-C., 2006. Advances in Cambrian stratigraphy and paleontology: Integrating correlation techniques, paleobiology, taphonomy and paleoenvironmental reconstruction. Palaeoworld 15, 217–222.
Zhu, M.Y., Zhang, J.M., Steiner, M., Yang, A.H., Li, G.X., Erdtmann, B.D., 2003. Sinian-Cambrian stratigraphic framework for-shallow- to deep-water environments of the Yangtze Platform: an integrated approach. Prog. Nat. Sci. 13, 951–960.
Zhu, R., Li, X., Hou, X., Pan, Y., Wang, F., Deng, C., He, H., 2009. SIMS U-Pb zircon age of a tuff layer in the Meishucun section, Yunnan, southwest China: Constraint on the age of the Precambrian-Cambrian boundary. Science in China Series D-Earth Sciences 52, 1385–1392.